Colloquium: Scaled particle theory and the length scales of hydrophobicity

Henry S. Ashbaugh

Department of Chemical and Biomolecular Engineering, Tulane University, New Orleans, Louisiana 70118, USA

Lawrence R. Pratt

Theoretical Division, Los Alamos National Laboratory, Los Alamos, New Mexico 87545, USA

(Published 30 January 2006)

Hydrophobic hydration plays a crucial role in self-assembly processes over multiple length scales, from the microscopic origins of inert gas solubility in water, to the mesoscopic organization of proteins and surfactant structures, to macroscopic phase separation. Many theoretical studies focus on the molecularly detailed interactions between oil and water, but the extrapolation of molecular-scale models to larger-length-scale hydration phenomena is sometimes not warranted. Scaled particle theories are based upon an interpolative view of that microscopic↔macroscopic issue. This Colloquium revisits the scaled particle theory proposed 30 years ago by Stillinger [J. Solution Chem. **2**, 141 (1973)], adopts a practical generalization, and considers the implications for hydrophobic hydration in light of our current understanding. The generalization is based upon identifying a molecular length, implicit in previous applications of scaled particle models, which provides an effective radius for joining microscopic and macroscopic descriptions. It will be demonstrated that the generalized theory correctly reproduces many of the anomalous thermodynamic properties of hydrophobic hydration for molecularly sized solutes, including solubility minima and entropy convergence, successfully interpolates between the microscopic and macroscopic extremes, and provides new insights into the underlying molecular mechanisms. The model considered here serves as a reference for theories that bridge microscopic and macroscopic hydrophobic effects. The results are discussed in terms of length scales associated with component phenomena. In particular, first there is a discussion of the microscopic-macroscopic joining radius identified by the theory; then follows a discussion of the Tolman length that describes curvature corrections to a surface area model of hydrophobic hydration free energies and the length scales on which entropy convergence of hydration free energies are expected.

DOI: 10.1103/RevModPhys.78.159 PACS number(s): 87.10.+e, 82.70.Uv, 87.15.−v

CONTENTS

I. INTRODUCTION: THE CENTRAL PUZZLE OF HYDROPHOBIC HYDRATION

The adage "oil and water don't mix" is a truism that underlies many phenomena of the aqueous environment, including surfactant assembly, folding of globular proteins, biological membrane formation, and the fate of pollutants in nature. But if one examines the interaction of hydrophobic substances with water more closely, one sees that the actual situation is more subtle. For example, many soluble proteins are globular at one temperature but unfold upon both heating and cooling. Simpler examples are the solubilities of inert gases in water, shown in Fig. 1, and contrasted with solubility of these gases in a typical organic solvent (cyclohexane). The temperature variations shown there are opposite for those two solvents, and the nonmonotonic behavior of the aqueous solubilities as a function of temperature is not expected on the basis of solubilities in cyclohexane. These distinctions between water and organic solvents are generic and are a central puzzle of hydrophobic hydration.

The ability to reproduce these temperature signatures from basic principles is essential for understanding the functional temperature ranges of biophysical structures and of aqueous phase nanotechnology designed by analogy with the molecular machinery of biophysics. An important aspect of these puzzles is that the hydrophobic temperature signatures are strongly affected by the spatial length scales of the hydrophobic solution structures.

The identification of a particular length scale has been a primary feature of recent discussions of hydrophobic effects (Lee, 1985; Lum *et al.*, 1999), though the length scales noted in those two cases were different from each other. It is interesting, therefore, to consider length scale issues more broadly. We can start by noting the classic suggestion of Egelstaff and Widom (1970) for a length scale characteristic of a liquid in coexistence with a dilute vapor phase, namely, the product of the liquid-vapor interfacial tension γ and the isothermal compressibility of the liquid $\kappa_T \equiv -(1/V)(\partial V/\partial p)_T$, where V is the volume of the system and p is the pressure. Since p has the dimensions of [energy/volume] and γ the dimensions of [energy/area], the combination $\gamma\kappa_T$ has the dimension [length]. The original argument supporting this suggestion was physical, heuristic, and our discussion below of the scaled particle theories will shed some additional light on this length scale. It was immediately observed, however, that away from a critical region the product $\gamma\kappa_T$ exhibited limited variation, though γ and κ_T could differ by two orders of magnitude from liquid to liquid.

Figure 2 shows that the temperature dependence of

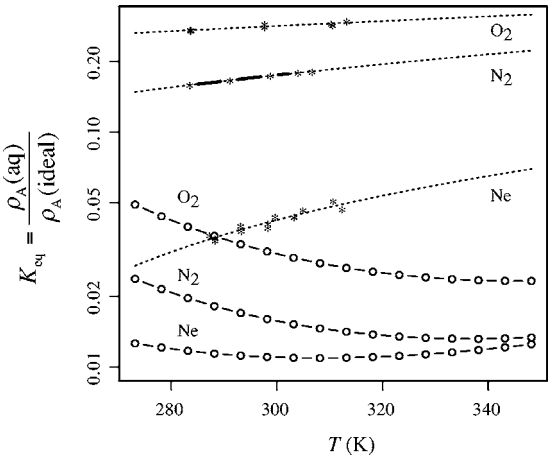

FIG. 1. Solubility of several inert gases in water and cyclohexane relative to the dilute gas phase expressed as the Ostwald partition coefficient following from Eq. (1), as a function of temperature at one atmosphere total pressure. The circles and interpolating solid lines are the data for liquid water as a solvent; the stars and the fitted dotted lines are for cyclohexane. Note that in the low-temperature region, these results for the two solvents have slopes of opposite sign. These solubility ratios are expected to increase in higher-temperature regions where the density of either solvent is decreasing and the distinctions between gas and liquid phase diminish.

$\gamma\kappa_T$ is qualitatively different for liquid water than it is for typical organic solvents. This qualitatively different behavior is mostly ascribable to the fact that the compressibility of liquid water displays a minimum at 46 °C. κ_T decreases with increasing temperature for temperatures lower than this, and has a smaller net variation over this temperature domain compared to the other solvents.

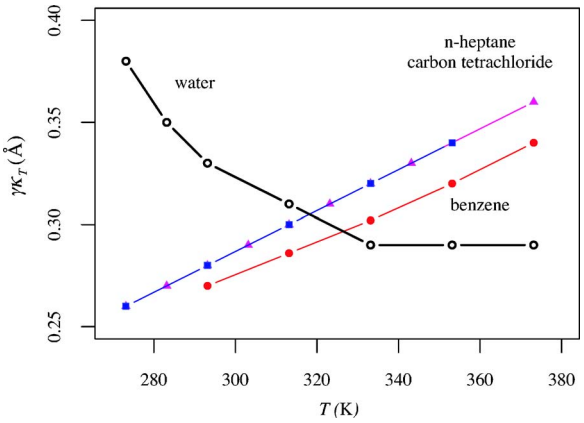

FIG. 2. (Color online) Product of the liquid-vapor surface tension γ and the isothermal compressibility $\kappa_T \equiv -(1/V)(\partial V/\partial p)_T$ for several liquid solvents at low temperatures so that the density of the coexisting vapor is low. Even though the individual factors differ substantially in magnitude, this product is a length characteristic of the liquid, accessible on the basis of macroscopic measurements, and can be taken as proportional to a molecular correlation length. The interesting observation here is that the temperature dependence of this correlation length is qualitatively different for liquid water than for the organic solvents.

Though liquid water is less compressible than most other liquids, the liquid-vapor surface tension is higher for water than for the other cases. This exemplifies the point that the product $\gamma\kappa_T$ has smaller variations than do the individual factors. Still, liquid water is distinguished from liquids generically by peculiar temperature dependences.

Analyzed on the basis of classical thermodynamics, these peculiar temperature dependences imply entropic stabilization of conformations and assemblies of hydrophobic solutes in aqueous solutions. These entropic effects can be appreciated qualitatively by asking why cold-unfolded proteins organize and order themselves upon heating. A qualitative start toward answering this question is to recognize that such an entropy question should also consider the water matrix. Thus ordering of a protein structure with increasing temperature can be balanced with disordering of the solution so that the entropy of the system increases with increasing temperature, as it must according to thermodynamic principles.

The theoretical description of hydrophobic effects has recently progressed markedly, and understanding of the entropic interactions that stabilize micelles, membranes, soluble proteins, and hierarchical biomolecular aggregations in aqueous solutions has similarly advanced. It is now recognized that scaled particle theories, which are discussed in detail in Sec. II, can properly describe primitive hydrophobic effects associated with the hydration of simple monatomic species. Scaled particle theories identify—tentatively at first, but firmly as information accumulates—a length separating microscopic from macroscopic descriptions of hydration structure. This establishes a radius at which microscopic and macroscopic descriptions of hydration structure can be effectively joined. Together with primitive constitutive information specific to liquid water, recognition of this joining radius provides an effective description of hydrophobic effects for mesoscale aqueous structures.

This Colloquium traces those advances, specifically by laying out the basic view generalizing applications of scaled particle approaches. We establish the microscopic-macroscopic joining length, discuss the length—analogous to the Tolman length [cf. Eq. (8) below]—associated with curvature corrections of a surface area model of hydrophobic hydration free energies, and finally examine the length scales on which entropy convergence of hydration free energies are expected.[1]

A. Hydrophobicity and amphiphilic solutes

Hydrophobic phenomena usually do not occur in isolation from other interaction effects. The solutes that motivate the study of hydrophobic effects are typically molecularly complicated, water-soluble, amphiphilic chain molecules—molecules that are part hydrophobic and part hydrophilic. Soluble protein molecules are examples.

Researchers studying these systems have been comfortable, however, with a hydrophilic-hydrophobic dichotomy. It is common to identify contributions to the hydration free energy above and beyond obvious hydrophilic interactions as hydrophobic effects (Pratt, 1998). This is particularly true if the temperature dependences of the complementary hydrophobic interactions are also distinctive (Spolar *et al.*, 1989; Spolar and Record, 1994). A helpful review of hydrophilic electrostatic interactions involved in protein molecular structure with an emphasis on the multiple length scales involved appeared recently (Simonson, 2003). The present discussion emphasizes model solutes, inert excluded volume models that permit the study of hydrophobic effects exclusively. Gases that are sparingly soluble in water, and small hydrocarbon molecules, can be brought into correspondence with hard-core molecular models. These models permit precision in isolating the temperature signatures that are the target of studies of hydrophobic effects.

B. Entropic and enthalpic driving forces

Phase changes are controlled by differences in free energies, which in turn can be separated into an entropy difference and an enthalpy difference. For many systems the solubilities can be understood principally in terms of the enthalpies; in fact, such systems are called *regular solutions*. Hydrophobic hydration, however, defies such a simple explanation. High-precision calorimetric studies show that unfavorable entropy changes dominate the room-temperature hydration free energies and are only partly compensated by favorable enthalpy changes. Not only that, but the entropies and enthalpies of hydrophobic hydration are strongly temperature dependent. The negative entropy difference rises rapidly with temperature leading to the reversed situation with an unfavorable enthalpy dominating the free energy and partly compensated by a favorable entropy change. The resulting solubilities of nonpolar gases are nonmonotonic, exhibiting solubility minima in the range 310–350 K; for examples, see Fig. 1. Analogously, proteins undergo hot and cold denaturation (Brandts, 1964; Franks and Hatley, 1991) as noted above, while ionic and nonionic surfactants display a minimum in their critical micelle concentrations with respect to temperature (Chen *et al.*, 1998a, 1998b), pointing to a common underlying mechanism with the solubility behavior of nonpolar species.

C. Temperature convergence of hydration entropies

The experimental entropy changes for a range of hydrophobic solutes intersect at small values of entropy differences in the region $T \approx 400$ K. Critical examples are presented in Fig. 3. The coincidence of these entropy-convergence temperatures for hydrocarbons

[1]Entropy convergence will be defined and exemplified in Sec. I.C and Fig. 3, and extensively discussed in this Colloquium, but particularly in Sec. III.E. Briefly, it is the experimental observation for many hydrophobic solutes that the entropy changes upon hydration approach a common value near zero in a narrow temperature regime, $T \approx 400$ K.

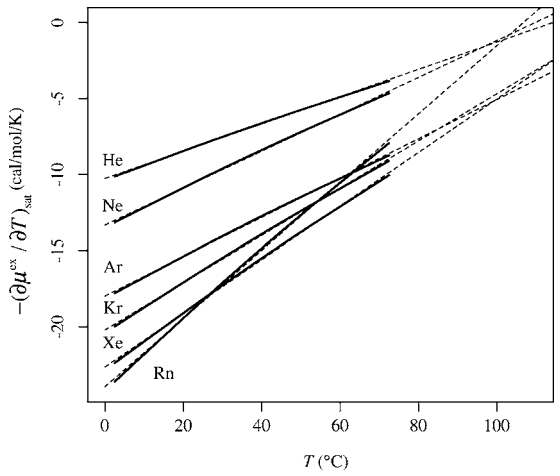

FIG. 3. Examples of the entropy-convergence phenomenon for noble gases dissolved in water. Results obtained from Ostwald coefficient results as a function of temperature, following Eq. (1), at one atmosphere total pressure. The bold solid curves are the data plotted up to 70 °C (Clever 1979a, 1979b, 1980); the dashed lines are fitted linear models. Results are available over a broader range for many cases, but this display adopts a common temperature range and gives an indication of the accuracy of the linear behavior. Radon (Rn) is clearly a special case, perhaps because of the strength of water-Rn dispersion interactions and the greater solubility of Rn. It is clear here that there is some variation of intersection ("convergence") temperatures. This variation is probably less evident in solubilities of small hydrocarbons that are more common as biophysical model systems, perhaps because of the better commonality of fundamental sizes and interaction strengths among those solutes.

with comparable behavior in protein unfolding has been used as empirical justification for the hydrophobic core model for protein folding and has influenced the interpretation of biomolecular assembly (Privalov, 1979; Baldwin, 1986; Privalov and Gill, 1988; Murphy *et al.*, 1990; Lee, 1991; Muller, 1993; Makhatadze and Privalov, 1995). But in the complex context of soluble protein molecules, the clear relevance of entropy convergence can be questioned (Robertson and Murphy, 1997).

D. Contrast of theories: From icebergs to scaled particle theories

It has been traditionally argued that these hydrophobic entropy effects stem from orientational constraints on water molecules in the hydration shell of nonpolar solutes, constraints that maintain the integrity of a hydrogen-bonding network forming cagelike structures or microscopic *icebergs* (Frank and Evans, 1945). Experimental probes of the local structure of water proximal to purely nonpolar solutes are scarce and hampered by the low solute concentrations attainable. The structures that have been studied by neutron- and x-ray scattering techniques suggest that while water adopts orientational preferences in the hydration shell of nonpolar moieties, the solute-induced structure is more disordered than in ice or clathrate hydrates (Broadbent and Neilson, 1994; DeJong *et al.*, 1997; Filipponi *et al.*, 1997; Bowron *et al.*, 1998a, 1998b). Theoretical studies of the impact of local clathrate formation about krypton in water concur with the experimental evidence that literal clathrate structures would be significantly more ordered than the water molecules in the immediate environment of Kr(aq) in liquid solution. For that reason, clathrate structures are improbable contributors to hydration thermodynamics (Ashbaugh *et al.*, 2003).

1. Empirically parametrized models

In contrast to historical views, a theme of modern theories of hydrophobic hydration is to exploit experimentally secured information on liquid water to describe the solutions of interest. The scaled particle theories (Stillinger, 1973; Pierotti, 1976) are examples of such an approach. Because temperature dependences are of primary interest, it is natural to insist that temperature dependences of any parameters be understood clearly, perhaps obtained from a separate experiment (Graziano and Lee, 2003). When experimental information ran out, modelers turned to simulation "data." For example, Pratt and Pohorille (1992, 1993) utilized simulations to fill in the outlines of scaled particle theories and demonstrated that the low solubility of atomic solutes in water arises from the narrow distribution of cavity-opening fluctuations in water. Utilizing an information theoretic approach, Hummer *et al.* (1998, 2000) then took the further step of providing a quantitative link between the microscopic density fluctuations determined from water oxygen pair correlations and the hydration free energies of hard solutes. Those results established a connection to the Pratt-Chandler theory (Pratt and Chandler, 1977) and its Gaussian field interpretation (Chandler, 1993; Lum *et al.*, 1999).

More importantly, the information theoretic model implicated the unusual equation-of-state properties of water as a dominant factor in hydrophobic hydration, differentiating water from other common solvents. As one example, the information theoretic model provided a facile description of the enhanced solubility of nonpolar species in D_2O compared to H_2O as a result of differences in the isothermal compressibilities of these isotopic alternative forms of water (Hummer *et al.*, 2000). Another example is the analysis of hydrophobic solubility in deeply supercooled water (Paschek, 2005).

2. Larger length scales and surface free energies

The empirical involvement of the equation of state brings us back to the length $\gamma\kappa_T$ of Fig. 2 because of the involvement of the measured isothermal compressibility with its specific temperature dependence. But the product $\gamma\kappa_T$ also involves the surface tension γ, and the surface tension has been invoked in empirical correlations connecting measurable properties of liquid water and hydrophobic effects. Years ago, however, Tanford (1979) pointed out the large discrepancy between the measured water-hydrocarbon interfacial tension and the effective microscopic surface tensions obtained from hydrocarbon

solubility data. A correspondence between macroscopic and microscopic surface tensions has been contentious because of their fundamentally different temperature dependence.

More recent examples of the distinction between molecular and macroscopic hydrophobic interactions are found in measurements of the long-range attractive force between macroscopic hydrophobic surfaces (Israelachvili and Pashley, 1982; Pashley *et al.*, 1985; Christenson and Claesson, 1988) that have not been explained on the basis of molecular hydrophobic effects. Vibrational sum-frequency spectroscopy suggests that the hydrogen bonding of water molecules is weaker at macroscopic water-carbon tetrachloride and water-hexane interfaces than near individual hydrophobic species dissolved in water (Scatena *et al.*, 2001). The lack of a definitive interpretation of these surface force measurements, and of the changes in water energetics at macroscopic interfaces, underscores the need for a quantitative theory beyond molecular hydrophobic effects. In general, the need for a unified, quantitative description of both molecular and macroscopic hydrophobic phenomena arises because hydrophobic driving forces play an important role in self-assembly on multiple length scales and from the fact that quantitative descriptions of these driving forces are derived from molecular solubility data, macroscopic interfacial tension measurements, or interpolations of these quantities (Hermann, 1977; Tanford, 1979; Sharp *et al.*, 1991; Ashbaugh *et al.*, 1999; Gallicchio *et al.*, 2000; Ashbaugh and Paulaitis, 2001).

Lum *et al.* (1999) suggested bridging these disparate length scales by incorporating a Gaussian field theory for molecular-level fluctuations with mean-field theory for larger-scale structures ultimately responsible for macroscopic phase transitions. Their approach successfully predicts many of the thermodynamic anomalies characteristic of small-molecule hydration, and goes further, predicting the onset of long-range hydrophobic forces between surfaces as a result of an aqueous liquid-vapor phase transition in confined geometries. Indeed, surface force apparatus studies of the long-range hydrophobic interaction (Christenson and Claesson, 1988) and simulations of water confined between repulsive oblate ellipsoids observed cavitation between nonpolar surfaces (Huang *et al.*, 2003), consistent with theoretical predictions. Mean-field modeling and simulations of methane clusters, however, suggest that when ubiquitous attractive interactions between water and hydrophobic surfaces are taken into account, surface and confinement-induced local structural changes are suppressed (Ashbaugh and Paulaitis, 2001; Truskett *et al.*, 2001; Chau, 2003; Dzubiella and Hansen, 2003; Zhou *et al.*, 2004; Ashbaugh *et al.*, 2005; Choudhury and Pettitt, 2005; Li *et al.*, 2005). Moreover, experiments on the effects of electrolyte addition and degassing on the range of surface forces, and the stability of surfactant-free aqueous emulsions, challenge the theoretical predictions (Kokkoli and Zukoski, 1998; Considine *et al.*, 1999; Pashley, 2003; Pashley *et al.*, 2005).

3. Scaled particle theories for microscopic-macroscopic interpolation

A conceptual basis for unifying molecular and macroscopic hydrophobic hydration can be found in scaled particle theory (SPT). Over 30 years ago, Stillinger (1973) presented an influential paper on the application of the classic SPT of Reiss (Reiss *et al.*, 1959; Reiss, 1965, 1977; Pierotti, 1976) to the hydration thermodynamics of purely excluded volume solutes. The purpose of that paper was, in part, to illuminate the pitfalls and difficulties in applying classic SPT, originally developed for hard-sphere fluids, to aqueous solvents (Ben-Naim and Friedman, 1967). In doing so, Stillinger opened new avenues of inquiry into hydrophobic hydration within the context of SPT. Nevertheless, direct exploration of the validity and consequences of Stillinger's revised theory have been rare (Pratt and Pohorille, 1992, 1993). We now revisit SPT and critically discuss its implications in light of our current understanding of hydrophobic hydration. We demonstrate that the revised SPT reproduces many of the characteristic thermodynamic signatures of molecular hydrophobic effects and can be used to extend the results of molecular simulations of small hard hydrophobic solutes in water to mesoscopic and macroscopic surface hydration. The present analysis provides insights into the differences and similarities for hydrating molecular and macroscopic surfaces. In addition, we examine the validity of surface area correlations commonly used in biophysical models for hydration thermodynamics over a range of length scales, as well as the origins of entropy-convergence behavior at molecular length scales and how solute size moderates the convergence temperature.

II. A PRIMER ON SCALED PARTICLE THEORY

The particle density $\rho_A(\mathrm{aq})$ of a dilute hydrated solute A in solution is conveniently expressed as

$$\rho_A(\mathrm{aq}) = \rho_A(\mathrm{ideal})\exp[-\mu_A^{\mathrm{ex}}(\mathrm{aq})/kT], \tag{1}$$

where $\rho_A(\mathrm{ideal})$ is the molecular number density of the coexisting gas phase treated as ideal. Thus the excess chemical potential, μ_A^{ex}, is central to resolving the aqueous solubility of the solute. The ratio of dissolved to ideal gas densities is also called the Ostwald partition coefficient $K_{\mathrm{eq}}=\rho_A(\mathrm{aq})/\rho_A(\mathrm{ideal})$. Considering Fig. 1 again, A=Ne is an example, and the density of Ne dissolved in water is about 1% of the gas density at $T=25\,^{\circ}\mathrm{C}$ and one atmosphere total pressure.

Let us now confine our discussion to impenetrable hard-sphere solutes, which we give a radius R. To make this more concrete, let us characterize the position of a water molecule by the oxygen center, and let the solvent-accessible radius R be the distance of closest approach between the solute center and a water oxygen. The solvent-accessible radius is usually taken as the sum of a van der Waals radius of a water molecule and the radius of the hard-sphere solute, i.e., $R=(\sigma_{\mathrm{WW}}+\sigma_{\mathrm{AA}})/2$. The ratio of densities is then just the ratio of volumes

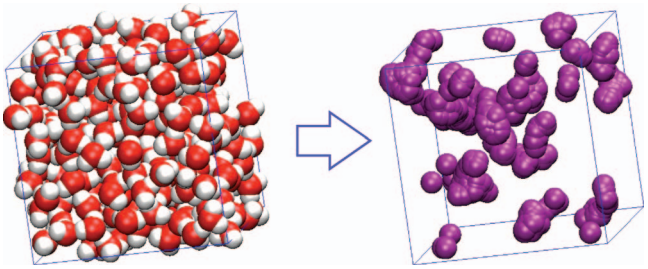

FIG. 4. (Color) The box on the left shows a configuration of water molecules taken from a simulation of liquid water at the density of the liquid in coexistence with vapor at 300 K. Oxygen atoms are red and hydrogen atoms are silver. The box on the right shows hard spheres of diameter 2.8 Å that can be successfully placed into the configuration on the right without overlap of the van der Waals volume of the water molecules. The insertion probability p_0 is determined as the volume accessible to a center of a purple sphere divided by the geometric volume of the box. See also Pratt, 1998.

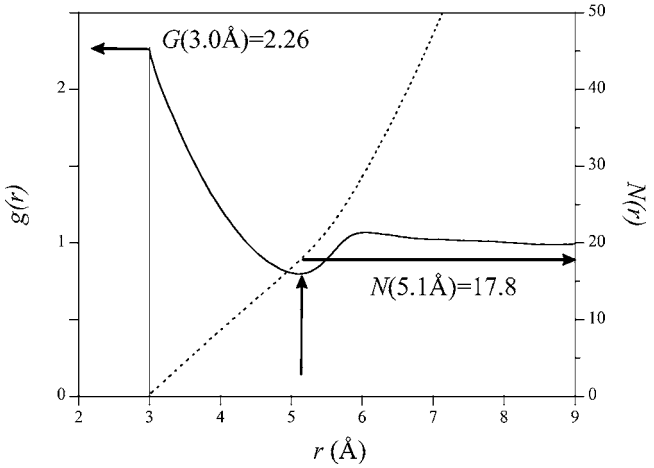

FIG. 5. Cavity-water oxygen radial distribution function for a $R=3$ Å cavity at $T=300$ K. The contact value, defined as $G(R)=\lim_{r\to R_+} g(r)$, is about 2.3. The thin solid curve indicates the radial distribution function, while the dotted curve indicates the radial integral $N(r)=\int_0^r \rho_W g(\lambda) 4\pi\lambda^2 d\lambda$. The occupation of the first hydration shell, corresponding to the first minimum in $g(r)$ at 5.1 Å, is 17.8 water molecules, as indicated by the thick horizontal line. Note that the first minimum, which physically discriminates between first and succeeding hydration shells, is mild and structuring of outer hydration shells is weak (Pratt and Pohorille, 1993). These features are in qualitative agreement with the predictions of the Pratt-Chandler theory (Pratt and Chandler, 1977), though that theory has been substantially amended (Pratt, 2002).

into which a solute might be placed. This in turn is equal to the insertion probability $p_0(R)$, the probability that a sphere of that radius randomly placed in water is devoid of water molecules. This follows directly from Widom's potential distribution theorem for species interacting with a hard potential (Widom, 1982; Pratt *et al.*, 1999).

The insertion probability is the fractional free volume offered by the solution—or the fractional *available* volume in a more specialized language attributed to Boltzmann (Stell, 1985),

$$p_0(R) = V_{\text{free}}/V_{\text{total}} = \exp[-\mu_A^{\text{ex}}/kT]. \tag{2}$$

For the hard-sphere case considered here, $K_{eq}=p_0(R)$. Figure 4 provides a visualization of the available volume V_{free}. Given a snapshot of a molecular configuration of liquid water—the left box in Fig. 4—V_{free} is the measure of the points at which a hard sphere could be successfully implanted. A successful placement of a hard-sphere solute particle identifies a molecular cavity in the solvent of a size at least as large as the hard sphere that was implanted. We flexibly use "cavity" to denote also that successfully placed hard-core solute because they are typically interchangable concepts. A graphic display of those successful placements thus yields a negative image—the right box in Fig. 4—of the molecular configuration from which the analysis started. V_{free} decreases with increasing cavity radius. This is true because some placements that are satisfactory for the solute radius of R will become unsatisfactory when the radius is increased to $R+\delta R$, but clearly no new successes are obtained in that way. Nevertheless, $p_0(R)$ is subsequently determined as an ensemble average over a large number of molecular configurations.

A direct computation of $p_0(R)$ may be performed by Monte Carlo simulations—as is suggested by Fig. 4—but that approach offers little insight. The scaled particle theory, in contrast, permits the construction of approximations with parameters determined by physical properties of water. It is based on the observation that the excess chemical potential of a hard-core solute is equal to the mechanical work needed to inflate a cavity of radius R in water, working against the thermal pressure exerted by the molecules at the cavity boundary. Let us define a quantity $G(R)$, the density of molecules at the boundary normalized to the bulk density ρ_W. $G(R)$ is the *contact value* of the radial distribution function shown in Fig. 5. Then the thermal pressure on the boundary is given by $kT\rho_W G(R)$, and the pdV work to expand the cavity, decreasing the volume of the fluid, is

$$\mu_A^{\text{ex}}(\text{aq}) = \int pdV = kT\int_0^R \rho_W G(r) 4\pi r^2 dr. \tag{3}$$

The name *scaled particle theory* derives from this expression (Reiss, 1965, 1977) since the solute is introduced by scaling up from a particle with a radius of zero to a final size of R.

A. Classic scaled particle theory

The substance of scaled particle theories, as a practical matter, is in the expressions and parametrizations for the function $G(R)$. How to parametrize $G(R)$ for the limiting cases of small or large distances is well known. For distances so small that only one solvent molecule could occur within the cavity boundary, the insertion probability is

$$p_0(R \to 0) = 1 - \frac{4\pi}{3}\rho_W R^3. \tag{4}$$

To relate this to $G(R)$, take the derivative of Eq. (3) and use Eq. (2) to obtain

$$G(R) = -\frac{1}{4\pi R^2 \rho_W}\left(\frac{\partial \ln p_0(R)}{\partial R}\right). \tag{5}$$

Carrying this out yields

$$G(R \to 0) = \frac{1}{1 - (4\pi/3)\rho_W R^3}. \tag{6}$$

The other simple limit is that of large R. Here the contact value can be represented as an asymptotic expansion in $1/R$,

$$G(R) \sim \sum_{j \geqslant 0} \frac{G_j}{R^j}. \tag{7}$$

Retaining contributions up to $j=2$ yields an expression familiar from classical thermodynamics as the force acting on the cavity surface (Reiss, 1965, 1977; Stillinger, 1973; Pierotti, 1976; Henderson, 2002),

$$kT\rho_W G(R) \sim p + \frac{2\gamma_\infty}{R} - \frac{4\gamma_\infty \delta}{R^2}, \tag{8}$$

where p is the liquid saturation pressure p_{sat}, γ_∞ is henceforth the surface tension of a flat interface that was denoted by γ above, and δ (Tolman, 1949) describes the initial curvature correction to the surface tension.[2] The coefficient G_3 is zero, so that the chemical potential is free of logarithmic contributions (Tully-Smith and Reiss, 1970; Stillinger and Cotter, 1971), though analyses of the possibility of logarithmic corrections are still of interest (Evans *et al.*, 2003, 2004). Higher-order terms in the asymptotic expansion are not generally available. Such considerations motivated Reiss *et al.* (1959) to truncate Eq. (7) after the initial curvature correction in order to develop a tractable, physically reasonable model for the contact values.

Evaluating the $j=0$ term in Eq. (7) with the measured equation of state, and the $j=1,2$ terms in the expansion by requiring that the microscopic and macroscopic limits meet smoothly at $\sigma_{WW}/2$, yields

$$G(R) = \begin{cases} \dfrac{1}{1 - (4\pi/3)\rho_W R^3}, & R \leqslant \sigma_{WW}/2 \\ \dfrac{p_{sat}}{kT\rho_W} + \left[\dfrac{2+\eta}{(1-\eta)^2} - \dfrac{2p_{sat}}{kT\rho_W}\right]\left(\dfrac{\sigma_{WW}}{2R}\right) + \left[-\dfrac{(1+2\eta)}{(1-\eta)^2} + \dfrac{p_{sat}}{kT\rho_W}\right]\left(\dfrac{\sigma_{WW}}{2R}\right)^2, & R > \sigma_{WW}/2, \end{cases} \tag{9}$$

where $\eta = (\pi/6)\rho_W \sigma_{WW}^3$ is the solvent packing fraction. Integration of this formula using Eq. (3) yields the excess chemical potential

$$\frac{\mu_A^{ex}}{kT} = \begin{cases} -\ln\left(1 - \dfrac{4\pi}{3}\rho_W R^3\right), & R \leqslant \sigma_{WW}/2 \\ \left[-\ln(1-\eta) + \dfrac{9\eta^2}{2(1-\eta)^2} - \dfrac{\eta p_{sat}}{kT\rho_W}\right] + \left[-\dfrac{3\eta(1+2\eta)}{(1-\eta)^2} + \dfrac{3\eta p_{sat}}{kT\rho_W}\right]\left(\dfrac{2R}{\sigma_{WW}}\right) \\ \quad + \left[\dfrac{3\eta(2+\eta)}{2(1-\eta)^2} - \dfrac{3\eta p_{sat}}{kT\rho_W}\right]\left(\dfrac{2R}{\sigma_{WW}}\right)^2 + \dfrac{\eta p_{sat}}{kT\rho_W}\left(\dfrac{2R}{\sigma_{WW}}\right)^3, & R > \sigma_{WW}/2. \end{cases} \tag{10}$$

Equations (9) and (10) constitute the classic SPT originally developed for the hard-sphere fluid (Reiss, 1965, 1977) but which was subsequently applied to water by Pierotti (1976) and Lee (1985). Fundamental difficulties arise in the application of classic SPT to water, however, including the erroneous prediction that the surface tension of water increases with temperature and passes through a maximum near $T=425$ K (Stillinger, 1973).

B. Revised scaled particle theory

The scaled particle model described above incorporates little molecular detail beyond the assigned van der Waals diameter σ_{WW} that might differentiate water from other solvents, and thereby limits the interpretation of complex hydration phenomena. To consider this problem more generally, we note that the insertion probability is formally expressed in terms of solvent structure by an inclusion-exclusion development (Reiss, 1965, 1977; Stillinger, 1973),

[2]The notation of Eq. (8) follows a typographic confusion widespread across the present problem. δ here is one-half the conventional Tolman length. Expressed more basically, the rightmost term in Eq. (8) is $(2\gamma_\infty/R^2)$ times the Tolman length δ. See Henderson (2002) and Moody and Attard (2001). This factor of 2 pops up again in Eq. (19). We thank J. R. Henderson for a discussion of this point.

$$p_0(R) = 1 - \langle n(R)\rangle_0 + \frac{1}{2}\langle n(R)[n(R)-1]\rangle_0 + \sum_{k\geqslant 3}\frac{(-1)^k}{k!}\langle n(R)[n(R)-1]\cdots[n(R)-k+1]\rangle_0, \tag{11}$$

where $n(R)$ is the number of oxygen atoms observed in a sphere of radius R. The inclusion-exclusion interpretation is that the term $\langle n(R)\rangle_0 = 4\pi\rho_W R^3/3 = V^{-1}\Sigma_{\text{molecules}} 4\pi R^3/3$ comes from the sum of the individual volumes excluded to the solute by each of the solvent molecules. Then $\langle n(R)[n(R)-1]\rangle_0/2$ corrects for otherwise overcounted pair overlaps of those individual molecular excluded volumes. This term vanishes if pair overlaps cannot occur, and operationally it vanishes because $n(R)$ is observed then to take values 0 or 1 only. Generally, however, that pair correction is nonzero but needs a further triple overlap correction, and so on. The kth term in this series vanishes for k exceeding the maximum number of solvent molecular centers that can be packed into a sphere of volume $4\pi R^3/3$ because then the probability of observing a k-tuple in the observation sphere is zero. Operationally, this is because $n(R)$ then only takes values 0, 1, 2, …, $k-1$, so the indicated average vanishes, and this is sufficient that all higher moments vanish too. It is on this basis that the limiting result Eq. (4) is established.

Evaluation of the general kth term requires knowledge of the k-body solvent oxygen distribution functions. These distribution functions are complicated, not available beyond the pair-distribution function, and in fact there has been only one investigation of terms beyond second order (Gomez *et al.*, 1999; Pratt *et al.*, 1999). Considering the small-cavity pair-correlation ($k=2$) contribution and the asymptotic macroscopic thermodynamic limits, Stillinger proposed a revised expression for the cavity contact value (Stillinger, 1973),

$$G(R) = \begin{cases} \dfrac{1 + (\pi\rho_W/R)\displaystyle\int_0^{2R} g^{(2)}(r) r^2 (r-2R)\,dr}{1 - (4\pi/3)\rho_W R^3 + (\pi\rho_W/R)^2 \displaystyle\int_0^{2R} g^{(2)}(r)(r^3/6 - 2R^2 r + 8R^3/3)\,dr}, & R \leqslant R^* \\ \dfrac{p_{\text{sat}}}{kT\rho_W} + \dfrac{2\gamma_\infty}{kT\rho_W R} - \dfrac{4\gamma_\infty\delta}{kT\rho_W R^2} + \dfrac{\lambda}{R^4}, & R > R^*, \end{cases} \tag{12}$$

where R^* is the radius at which $n=3$ correlations begin to contribute to the cavity insertion probability of Eq. (11). Here $g^{(2)}(r)$ is the oxygen-oxygen radial distribution function of liquid water. While the experimental pressure, surface tension, density, and solvent radial distribution function are employed directly, δ and λ are treated as adjustable parameters chosen so that the small cavity and macroscopic limits of the contact values join smoothly at R^*. This expression incorporates molecular information on the pair structure of water as well as the known macroscopic properties of bulk water and its interfacial behavior and therefore is expected to discriminate more sensitively between water (Ashbaugh and Paulaitis, 2001) and other solvents (Huang and Chandler, 2000a). Indeed, molecular simulations have demonstrated that Eq. (12) provides a description superior to the classic SPT expression in Eq. (9) of the solvent contact density for solutes several times larger than the solvent.

C. Scaled particle model revised on simulation results

Stillinger's revised SPT prediction for $G(R)$ relies on the assumption that multibody water correlations at intermediate, but molecule-sized, solute radii are adequately represented by the parameters δ and λ fitted at a radius R^*. Numerical experimentation (Pratt and Pohorille, 1992) with this parametrization shows that the revised SPT is sensitive to the parameter R^*. This parametrization might be improved by involving results over a range of radii, including solute sizes for which multibody correlations are significant. If Eq. (7) is taken mathematically as an asymptotic series, then using it for the smallest possible values of $1/R$ would be the best way to improve its accuracy. While the necessary multibody correlations are not readily available experimentally, hard-sphere solute chemical potentials can be investigated by direct evaluation of the insertion probabilities from molecular simulations of water. In the spirit of Stillinger's revised SPT, we interpolate between the chemical potential evaluated for molecular length scales from simulation and the asymptotic macroscopic thermodynamic formula

$$\mu_A^{\text{ex}}(R) = -kT \ln p_0(R)|_{\text{sim}} f(R) + \mu_A^{\text{ex}}(R)|_{\text{macro}}[1 - f(R)], \tag{13}$$

where $f(R)$ is a switching function equal to one below

R_{sim} and zero above R_{macro}, smoothly interpolating between these two limits. Presently we use a cubic spline interpolating function, though other reasonable functions yield essentially indistinguishable predictions. The macroscopic chemical potential, determined by integration of the macroscopic cavity expression Eq. (12), is

$$\mu_A^{ex}(R)|_{macro} = -\frac{4\pi kT\rho_W\lambda}{R} + \epsilon - 16\pi R\gamma_\infty\delta + 4\pi R^2\gamma_\infty + \frac{4\pi}{3}R^3 p_{sat}. \quad (14)$$

Rather than fitting the microscopic and macroscopic limits at a single point as in Eq. (12), the parameters δ,λ, and the integration constant ϵ are fitted to the simulation results between R_{sim} and R_{macro}. The contact correlation function is then determined by differentiation of the chemical potential [Eq. (5)]. An additional benefit of fitting Eq. (14) to the simulation insertion probabilities is that we do not have to evaluate numerically first and second derivatives of the simulated insertion probabilities, which become more statistically uncertain with increasing cavity size.

D. Computational implementation

The computational implementation follows standard procedures for sampling molecular configurations of liquid water and builds upon the original work of Pohorille and Pratt (1990) and Pratt and Pohorille (1992, 1993) in evaluating cavity statistics therefrom. Water configurations were generated using Monte Carlo simulations in the canonical ensemble (Frenkel and Smit, 2002). Bulk water was modeled using 268 SPC/E water molecules with periodic boundary conditions (Berendsen *et al.*, 1987). The empirical SPC/E, or "simple-point-charge/extended model," is composed of Lennard-Jones interactions between oxygen centers of water molecules and electrostatic interactions describing water molecule orientations, and thus hydrogen positions. The SPC/E model was chosen here because it provides accurate representations of the structure, equation of state, and interfacial tension of liquid water over a broad range of temperatures (Alejandre *et al.*, 1995; Hura *et al.*, 2003). Lennard-Jones potential interactions were evaluated by smoothly truncating the potential based on the separation of water oxygen atoms between 9.5 and 10 Å, while longer-ranged electrostatic interactions were calculated using Ewald summation with conducting boundary conditions (Frenkel and Smit, 2002). Simulations were carried out from $T=260$ to 470 K in 10 K increments at the experimental liquid density along the saturation curve and into the supercooled regime (Hare and Sorensen, 1986). After an equilibration phase of at least 10^5 Monte Carlo passes (in which one pass corresponds to one attempted move per water molecule with 30% move acceptance), 5×10^6 Monte Carlo production passes were carried out for analysis of thermodynamic averages. After each 50 Monte Carlo passes, 10^5 particle insertions were attempted to estimate $p_0(R)$, so that a total of 10^{10} insertions were attempted at each temperature. Statistical uncertainties were determined by grouping results into block averages over 10^6 Monte Carlo passes each.

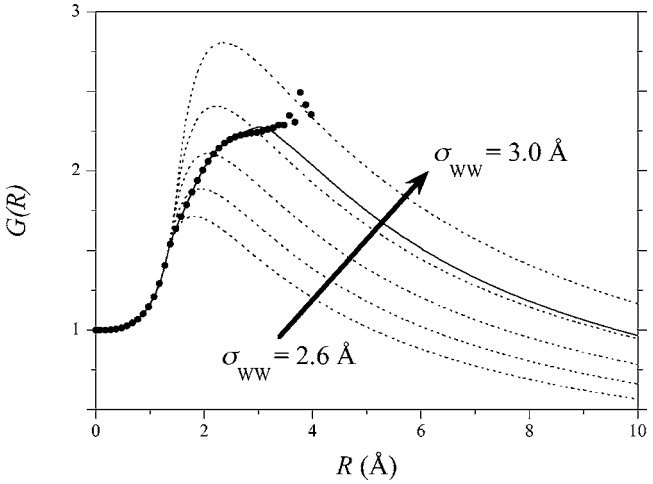

FIG. 6. Cavity contact values for water at $T=300$ K at liquid saturation conditions. The points are obtained by differentiation of the simulated cavity insertion probabilities. The dashed lines are obtained from Reiss's original SPT predictions for a hard-sphere solvent, Eq. (9), using effective hard-sphere diameters for water over the range from $\sigma_{WW}=2.6$ to 3.0 Å in 0.1 Å increments. The solid curve is obtained by differentiation of the revised SPT predictions, Eq. (14), fitted to the simulation results between $R_{sim}=2.5$ Å and $R_{macro}=3.5$ Å.

III. APPLICATION TO HYDROPHOBIC HYDRATION

A. Cavity contact values and the micro-macro joining boundary

The cavity contact values at $T=300$ K are shown in Fig. 6. Beginning at a value of 1 at zero radius, the cavity contact density increases with increasing R. Simulation values of $G(R)$ display a plateau near 3 Å. Just beyond this radius, the simulation results for $G(R)$ become progressively noisy owing to poor sampling of infrequent large cavity fluctuations. Detailed calculations for specific values of R greater than 3 Å (Ashbaugh and Paulaitis, 2001) have established that this is indeed the region of a maximum in $G(R)$, and that $G(R)$ is qualitatively described by Stillinger's revised scaled particle model. A dominating observation is that this curve imposes a nonarbitrary definition of a length scale for the present problem: the radius R_{max} at which $G(R)$ is maximal. Solutes with smaller radii are identified as intrinsically microscopic in scale. The description of larger solutes can be built from a macroscopic perspective. An interpolative strategy covering intermediate-sized, such as that adopted here, is likely to be effective if the region at which the molecular and macroscopic expressions are joined encompasses R_{max}. The revised SPT fit, determined by differentiation of Eq. (13) fitted to the simulation insertion results between $R_{sim}=2.5$ Å and $R_{macro}=3.5$ Å, extends $G(R)$ to R larger than observed directly.

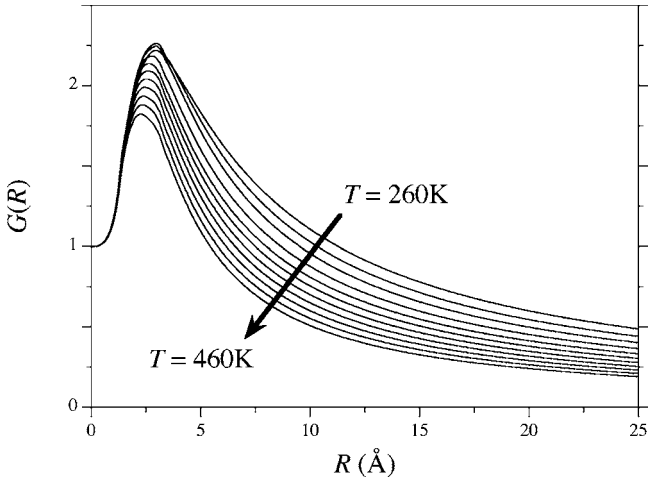

FIG. 7. Cavity contact function for water along the liquid saturation curve for several temperatures, as determined by the revised SPT, Eq. (13), with $R_{\mathrm{sim}}=2.5$ Å and $R_{\mathrm{macro}}=3.5$ Å. Results are shown over the range from $T=260$ to 460 K in 20 K increments. Notice that the length defined by the maximum of this curve decreases with decreasing density (following increasing temperature) along the saturation curve. This is qualitatively consistent with the data of Fig. 2.

The revised SPT result places the maximum contact density at $R=3.0$ Å, where $G(R)\approx 2.3$. Solutes of this size are candidates for "most hydrophobic" because the pressure exerted by the solvent is largest in this case. Figure 5 shows the distribution of oxygen atoms radially from such a solute.

1. Comparison with classic scaled particle theory

The classic SPT predictions for the contact values [Eq. (9)] are in qualitative agreement with the simulation and revised SPT results (Fig. 6). Classic SPT predicts a maximum in the contact density, followed by a decrease to values below the bulk density of water with increasing cavity radius. The quantitative agreement is poor, however, even if the effective diameter σ_{WW} of water is treated as an adjustable parameter. Classic SPT predicts that the maximum in $G(R)$ is shifted to smaller radii, $R\approx 2$ Å. Water has an open structure favoring larger cavities at these packing fractions (Pohorille and Pratt, 1990; Pratt and Pohorille, 1992). The resulting maximum in the pressure acting on the solute surface, $kT\rho_{\mathrm{W}}G(R)$, is then shifted out to larger cavity radii in the case of water.

If the objective of classic SPT is to reproduce the chemical potentials of solutes using Eq. (10) up to radii of $R\approx 3.3$ Å, encompassing the sizes of a number of nonpolar gases, a typical diameter σ_{WW} of water fitted to experimental data is 2.7 Å (Lee, 1985), though a more appropriate value based on the simulation results reported in Fig. 6 is 2.8 Å. In this case, the fitted radius of water splits the difference between the overprediction of $G(R)$ at intermediate radii by the classic SPT and the underprediction of $G(R)$ at radii close to the maximum solute size to balance out inaccuracies in the calculation of the chemical potential. The σ_{WW} assigned to water molecules is then a consequence of the fitting and does not contribute to the interpretation of the molecular signatures of hydrophobicity. Indeed, if we extend the predictions of classic SPT outside the range fitted for small solutes, we find the theory underpredicts the hydration free energies of mesoscopic cavities, and that a larger water diameter—$\sigma_{\mathrm{WW}}\approx 2.9$ Å—is required to match the drying observed in $G(R)$ (Fig. 6).

While the variation of this size parameter may seem small, the chemical potential depends on the integral of Eq. (3), and small differences in σ_{WW} significantly alter the predictions. Broadly viewed, this is the natural observation that a slight adjustment of boundary information in boundary-value problems can make large changes away from the boundary.

2. Temperature dependence of the micro-macro joining radius

Revised SPT predictions for $G(R)$ as a function of temperature are shown in Fig. 7. While the curves are qualitatively similar, the magnitudes of the contact values decrease with increasing temperature. Classic SPT fails to describe this temperature dependence of $G(R)$. Figure 7 also indicates that the length defined by the maximum of this curve decreases with increasing temperature, which is qualitatively consistent with the data in Fig. 2. In the following sections we use these revised SPT results to draw conclusions regarding the size and temperature dependence of the hydration of hydrophobic hard spheres.

The results of Fig. 7 shed some light on the length scale $\gamma_\infty\kappa_T$ discussed in Sec. I. Specifically, we can put together the crudest of models of the hydration free energies for the small-scale and large-scale problems, and in that way get a crude characterization of the length at which these different descriptions for $G(R)$ match. For the small scale—but not the smallest scale as in Eq. (4)—the information theory of Garde *et al.* (1996) and Pratt (2002) suggested $\beta\mu_{\mathrm{A}}^{\mathrm{ex}}\approx\langle n\rangle_0^2/2\langle\delta n^2\rangle_0$. If we evaluate everything on a macroscopic basis, then we obtain the crude estimate $G(R)\approx\beta/2\rho_{\mathrm{W}}\kappa_T$ from Eq. (5). For the large-scale problem, we use $\beta\mu_{\mathrm{A}}^{\mathrm{ex}}\approx 4\pi R^2\beta\gamma_\infty$, expecting that the pressure will be negligibly low in this case. Then $G(R)\approx\beta\gamma_\infty/R\rho_{\mathrm{W}}$. These two estimates match at the radius $2\gamma_\infty\kappa_T$. This dimensionally natural point should not be taken quantitatively in the present context because a slightly more general consideration immediately leads to another length, $\sqrt{kT/\gamma_\infty}$, that should be included. Other lengths will also arise, but the scaled particle approach does not require that we anticipate all those possibilities.

3. Dewetting for large cavities

Beyond the maximum, water pulls away from the cavity surface with increasing size. At $R\approx 10$ Å, the contact density equals the bulk density of water, decreasing further for larger cavities. In the limit $R\to\infty$, the contact value approaches $p_{\mathrm{sat}}/\rho_{\mathrm{W}}kT\approx 2\times 10^{-5}$ for water at T

=300 K, and the pressures here are sufficiently low that they do not influence the contact value for molecular and mesoscopic cavities at any of the temperatures considered.

This drying behavior was anticipated by Stillinger (1973) and has only recently been confirmed by molecular simulations in Lennard-Jones and aqueous solvents (Huang and Chandler, 2000a; Ashbaugh and Paulaitis, 2001). Surface drying has been previously interpreted in terms of an effective expulsion potential between water and the solute cavity (Hummer and Garde, 1998; Weeks *et al.*, 1998). In bulk water, the individual water molecules feel attractive interactions with other water molecules, and the average force on a water molecule in the bulk is zero. To approach a large solute, however, a water molecule must shed hydration partners and/or limit their configurations. This unbalances the interactions with the aqueous medium and gives rise to an additional repulsive force between a water molecule and the surface. If the solute is unable to compensate for these lost interactions to counter the cavity expulsion potential, water is repelled by the surface.

B. Physical relevance of hard-core model solutes to structural theories of hydrophobic effects

A successful generic description of liquids is obtained from van der Waals's separation of the intermolecular interactions into two parts, a repulsive part treated as volume exclusion and an attractive part treated perturbatively (Widom, 1967; Barker and Henderson, 1976; Lebowitz and Waisman, 1980; Chandler *et al.*, 1983). Physically expressed, van der Waals approaches are appropriate for the description of dense liquids because the disorder and high density can limit structural fluctuations to length scales associated with the variation of intermolecular repulsive interactions, which are small compared to the range of intermolecular attractive interactions. When attractive intermolecular interactions are weak on a thermal scale, that helps too since a van der Waals approach treats those interactions perturbatively. Repulsive interactions then present the first challenge to theories, and hard-core interactions are natural simple models for the excluded volume interactions. This is the argument for the physical relevance of hard-core model solutes to theories of hydrophobic effects (Pratt, 2002).

With this background, the most important physical observation on the large-R behavior of the $G(R)$ results of Fig. 7 is that those results would be expected to be sensitive to attractive solute-water interactions, if they were to be included. When R is large, the local density in the vicinity of the hard-sphere solute can be low, and the argument above (that fluctuations do not access the length scales comparable to the range of natural attractive interactions) does not apply. Simulation evidence does support the view that results can be sensitive to the inclusion of natural attractive interactions when the solution structures have length scales substantially greater than $R_{\max}$ (van Swol and Henderson, 1986; Henderson and van Swol, 1988; Ashbaugh and Paulaitis, 2001; Hummer *et al.*, 2001; Truskett *et al.*, 2001; Wallqvist *et al.*, 2001; Chau, 2003; Dzubiella and Hansen, 2003; Zhou *et al.*, 2004; Li *et al.*, 2005).

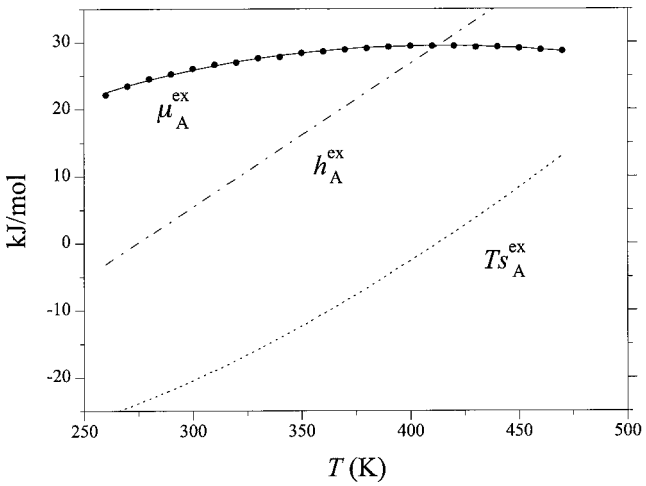

FIG. 8. Excess chemical potential, enthalpy, and temperature $\times$entropy of a methane-sized hard-sphere solute (R=3.3 Å) in water as a function of temperature along the saturation curve. The subscript A indicates the solute component, which in this case is CH_4 (methane). The points are the explicit simulation results for the chemical potential. Error bars are comparable in size to the points. The curves for the excess chemical potential, enthalpy, and entropy are labeled. The curves were determined under the assumption that the heat capacity is independent of temperature [Eqs. (15)].

Nevertheless, hard-core models of solute-water interactions serve as a valuable reference point for at least two reasons. A first reason is conceptual and reductionist. This simplified case has historically been considered as expressing the basic puzzle of hydrophobic effects. (The extent to which that is true is one of the issues addressed here.) Solving this basic puzzle enables specific cases to be described by combining what is understood for simpler cases. A second reason that hard-core models of solute-water interactions are valuable is that for R not too large the results should be less sensitive specifically to the case of physical interest. (Support for this view is noted at the appropriate places in the succeeding discussions.) From this point of view then the careful study of the large-R behavior of hard-sphere $G(R)$ assists in refining the description of intermediate-R behavior, including the region of the maximum corresponding to the most hydrophobic solutes.

C. Hydration thermodynamics of hydrophobic species: Temperature signatures and solubility minima

The hydration free energy of a methane-sized (R =3.3 Å) hard-sphere solute in water as a function of temperature along the saturation curve is shown in Fig. 8. The simulation results for the chemical potential pass through a maximum at $T\approx 400$ K, at which point the hydration entropy defined by $s_A^{ex}=-\partial\mu_A^{ex}/\partial T|_{sat}$ vanishes. To extract the enthalpy and entropy of hydrophobic hydration from the chemical potential, we assume that the

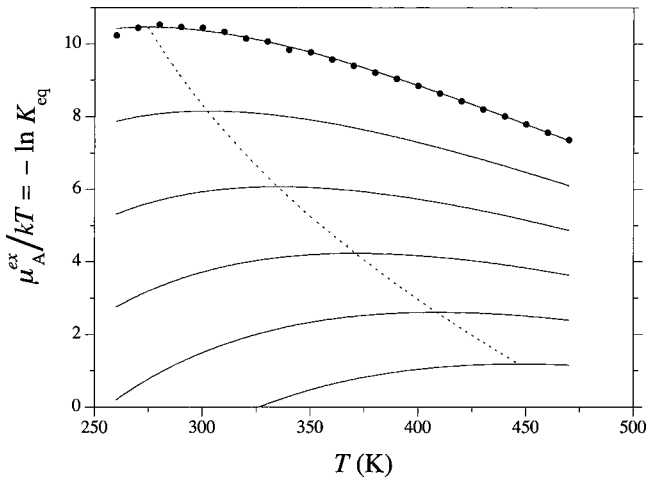

FIG. 9. Ostwald solubility, $-\ln K_{eq}=\mu_A^{ex}/kT$ [cf. Eq. (1) and following], modeled as in the van der Waals equation of state, $\mu_A^{ex}=[\mu_A^{ex}]_{HS}-2a_{AW}\rho_W$ for a 3.3 Å solute, as a function of temperature with increasing strength of attractive interactions. The points are simulation results from particle insertion probabilities. The solid curves are the solubilities for increasingly attractive interactions, $a_{SW}\geqslant 0$, proceeding from the top curve to the bottom curve. The dashed curve indicates the maxima in μ_A^{ex}/kT.

heat capacity $\partial h_A^{ex}/\partial T|_{sat}=T\partial s_A^{ex}/\partial T|_{sat}=c_A^{ex}(T)$ is independent of temperature. In this case, the hydration enthalpy, entropy, and free energy are

$$h_A^{ex}=h_A^{ex}(T_0)+(T-T_0)c_A^{ex}(T_0), \tag{15a}$$

$$s_A^{ex}=s_A^{ex}(T_0)+\ln\left(\frac{T}{T_0}\right)c_A^{ex}(T_0), \tag{15b}$$

$$\mu_A^{ex}=\mu_A^{ex}(T_0)+(T-T_0)[c_A^{ex}(T_0)-s_A^{ex}(T_0)]-T\ln\left(\frac{T}{T_0}\right)c_A^{ex}(T_0), \tag{15c}$$

respectively, and $\mu_A^{ex}(T_0)=h_A^{ex}(T_0)-T_0s_A^{ex}(T_0)$.

The enthalpy and entropy of hydration of the methane-sized hard-sphere solute are plotted together with the fitted free energy in Fig. 8. The hydration entropy is negative and unfavorable at room temperature (Kauzmann, 1959; Tanford, 1980; Blokzijl and Engberts, 1993). With increasing temperature the negative entropy changes sign, indicative of a positive heat-capacity increment. The entropy and heat capacity at $T=298$ K for the hard-sphere solute are −69.5 and 214 J/(mol K), respectively, which are in excellent agreement with the experimental values for the entropy and heat capacity of −66.7 and 209–237 J/(mol K) for methane at $T=298$ K (Rettich *et al.*, 1981; Ben-Naim and Marcus, 1984; Naghibi *et al.*, 1986; Lazaridis and Paulaitis, 1992). Over most of the temperature range considered, the hydration enthalpy is positive and unfavorable for hydration, in disagreement with the experimental enthalpy for methane of −11.5 kJ/mol at $T=298$ K, largely a result of the neglect of attractive interactions with water. The iceberg hypothesis of Frank and Evans (1945) suggested that local freezing of water in the vicinity of hydrophobic species contributes to the experimental negative hydration enthalpy. In the case of the methane-sized hard sphere though, the hydration enthalpy at $T=298$ K is 5.0 kJ/mol and is positive, contrary to the most common view that water molecules neighboring simple hydrophobic solutes make more effective, lower-energy hydrogen bonds than in the bulk!

1. Primitive effects of solute-solvent attractive interactions

The ratio of the chemical potential and kT dictates the Ostwald solubility as $\mu_A^{ex}/kT=-\ln K_{eq}$ from Eq. (1) and the following. This information for the methane-sized solute in water as a function of temperature is shown in Fig. 9. This quantity passes through a maximum near $T=280$ K, corresponding to a minimum in the solubility. This observation is in agreement with information theory (Garde *et al.*, 1999) and equation-of-state (Ashbaugh *et al.*, 2002) models of hard-sphere solubilities that link the solubility minimum to the density maximum at $T=277$ K for pure water. The solubility minimum corresponds to the point at which the enthalpy $h_A^{ex}=-T^2\partial(\mu_A^{ex}/T)/\partial T|_{sat}$ equals zero. Real nonpolar solutes display solubility minima at temperatures well above the density maximum, largely as a result of attractive interactions between the solute and water. These interactions, not included in the present simulations, can be included approximately by assuming they are proportional to the density of liquid water, as in the van der Waals equation of state. The resulting chemical potential is $\mu_A^{ex}=[\mu_A^{ex}]_{HS}-2a_{AW}\rho_W$ (Garde *et al.*, 1999). The effect of including solute-water interactions on the solubility is shown in Fig. 9. Increasing these interactions systematically shifts the minimum in $\ln K_{eq}$ out to greater temperatures, in agreement with the experimental observation of solubility minima at higher temperatures.

2. Temperature dependence of the heat-capacity difference

For the hard-sphere solutes, the simulation results shown in Fig. 9 have slightly more curvature at temperatures near the solubility minimum than predicted by Eq. (15). While the fit is accurate, the enhanced curvature suggests the heat capacity is not constant as assumed above, but is slightly larger at low temperatures. Indeed, this has been observed experimentally (Gill *et al.*, 1985) and is borne out by theoretical models of hydrophobic hydration as well (Hummer *et al.*, 2000; Silverstein *et al.*, 2001; Ashbaugh *et al.*, 2002). Nevertheless, the temperature dependence of the heat capacity is minor, and including it is a complication of secondary importance to the interpretations here. We therefore neglect it in our thermodynamic analysis.

3. Size dependence of hydration free energies

Figure 10 shows the chemical potential of hard spheres in water as a function of temperature with in-

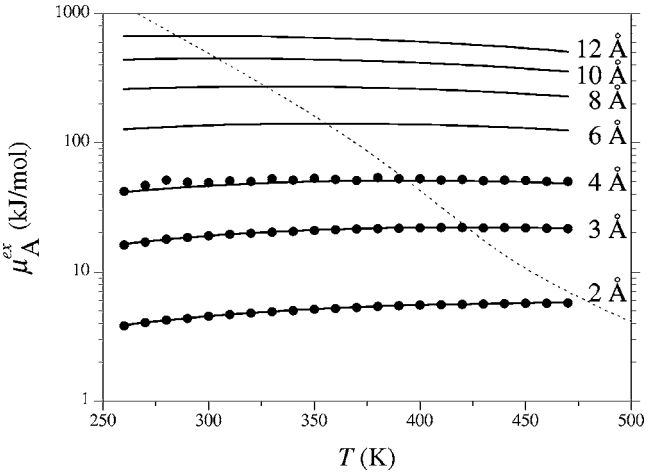

FIG. 10. Excess solute chemical potential as a function of temperature for solutes of varying size. The solid lines correspond to the revised SPT model. The solid circles correspond to molecular simulation results for the 2, 3, and 4 Å radius solutes. Estimated statistical errors are smaller than the plotting symbols. The dashed curve indicates the locus of chemical-potential maxima, where $s_A^{ex}=0$, with changing cavity size.

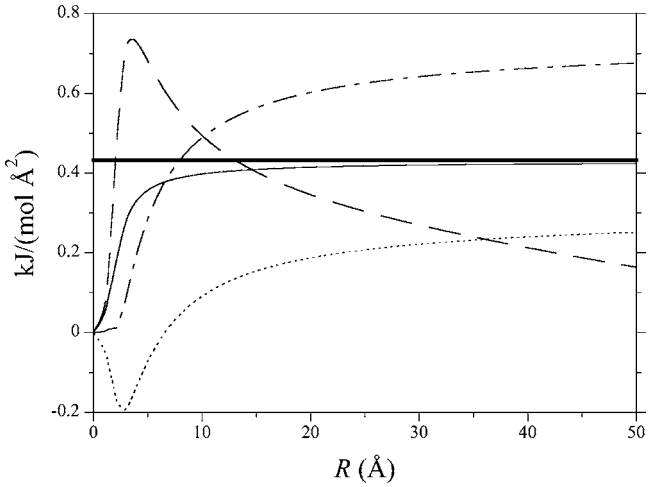

FIG. 11. Solvent-accessible surface (SAS) area derivatives of the hard-sphere solute hydration thermodynamics as a function of solute radius at $T=300$ K. The thin solid, long-short dashed, short dashed, and long dashed curves correspond to $\partial\mu_A^{ex}/\partial A_{SAS}$, $\partial h_A^{ex}/\partial A_{SAS}$, $T\partial s_A^{ex}/\partial A_{SAS}$, and $T\partial c_A^{ex}/\partial A_{SAS}$, respectively. The horizontal curve indicates the macroscopic surface tension for a flat surface.

creasing solute size. In the range of sizes shown, the maximum in the chemical potential shifts from temperatures greater than $T=470$ K, above the window of temperatures simulated for the 2 Å radius solute, to lower temperatures with increasing solute sizes. For cavities not much larger than 12 Å (not shown in the figure), the maximum falls below $T=260$ K, beneath the simulation window and the normal freezing point of water. Thus, for molecularly sized cavities, hydrophobic hydration is opposed by a negative entropy over most of the range of temperatures simulated. For mesoscopic and macroscopic cavities, however, this trend is reversed and hydration is favored by a positive dissolution entropy but is unfavorable as a result of a dominating positive enthalpy (discussed in the next section) dictated by the temperature dependence of the surface tension of water.

D. Surface contributions

To compare and correlate hydration free energies of a variety of species, it is common to calculate the free energy cost per unit area for hydrating nonpolar solute surfaces, also referred to as a molecular surface tension (Hermann, 1977; Tanford, 1979). This molecular surface tension, however, is generally not equal to the free energy of creating a macroscopic flat interface, in part due to curvature and structural differences between water at molecular and macroscopic interfaces. Nevertheless, SPT systematically interpolates the surface tension between these two length scale extremes and provides insight into their relationship (Huang and Chandler, 2000a; Ashbaugh and Paulaitis, 2001; Huang *et al.*, 2001).

Under the assumption that the pressure contribution to the hydration free energy is negligible, an excellent assumption for liquid water, the surface tension for hydration of a hard-sphere solute is obtained from the surface area derivative of the chemical potential (Ashbaugh and Paulaitis, 2001). This derivative depends, however, on the definition of the surface area. A natural choice for the solute area is defined by R, and is referred to as the solvent-accessible surface area $A_{SAS}=4\pi R^2$. Differentiating the chemical potential with respect to this surface area yields

$$\gamma_{SAS}(R)=\frac{\partial\mu_A^{ex}}{\partial 4\pi R^2}=\frac{1}{2}kT\rho_W G(R)R. \tag{16}$$

1. Entropic and enthalpic contributions to surface free energies as a function of radius

The solvent-accessible surface tension as a function of R at $T=300$ K is shown in Fig. 11. The surface enthalpy $\partial h_A^{ex}(T_0)/\partial A_{SAS}$, entropy $\partial s_A^{ex}(T_0)/\partial A_{SAS}$, and heat capacity $\partial c_A^{ex}(T_0)/\partial A_{SAS}$ are included in this figure. For small cavities, all the surface thermodynamic properties go to zero as $R\to 0$. With increasing size, the surface tension $\partial\mu_A^{ex}(T_0)/\partial A_{SAS}$ increases monotonically and approaches its asymptotic limit for a flat interface of $\gamma_\infty=0.432$ kJ/(mol Å^2)$=71.7$ dyn/cm. The other surface properties, most notably the heat capacity, approach their asymptotic plateaus more slowly with increasing R. As with surface tension, the surface enthalpy monotonically increases with increasing solute size. The surface entropy and heat capacity, on the other hand, vary in distinctly different ways for molecular and macroscopic surfaces, indicating changes in the mechanism of hydration (Southall and Dill, 2000). In particular, the surface entropy is initially negative beginning from $R=0$, consistent with the experimental thermodynamics of hydrophobic hydration for molecular solutes, reaches a minimum at $R\approx 3.3$ Å, and then increases, eventually becoming positive as expected from the temperature de-

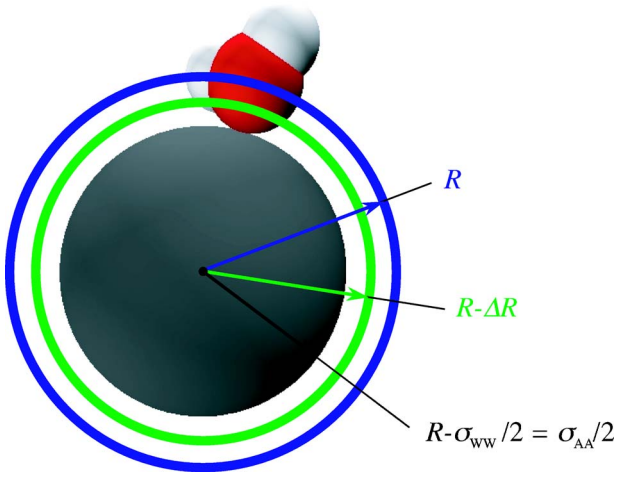

FIG. 12. (Color online) Alternative definitions of the surface for evaluation of the surface tension. The solvent-accessible surface (SAS) is defined by the distance of closest approach between the center of the cavity and the water-oxygen center R. $R-\Delta R$ locates a neighboring surface that might provide a curvature-corrected surface tension. The radius $R-\sigma_{WW}/2$ gives the van der Waals boundary at $\sigma_{AA}/2$.

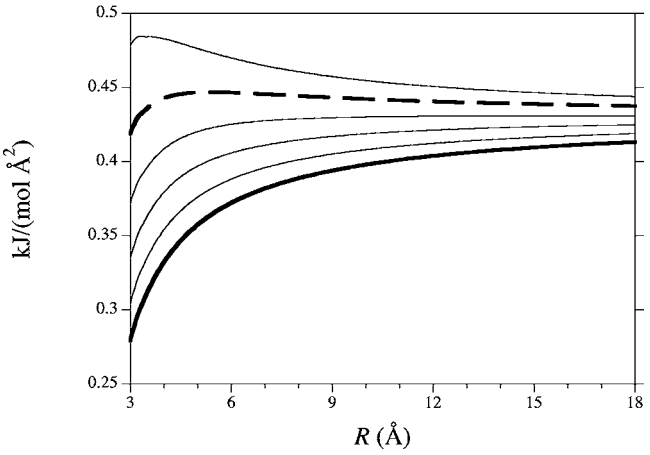

FIG. 13. Surface tensions referred to defined surfaces, displaced with respect to the solvent-accessible surface located at the radius R, for hydration of hard-sphere solutes as a function of solute size at $T=300$ K. The thick solid curve corresponds to the surface tension determined by the derivative with respect to the solvent-accessible surface (SAS) area [Eq. (16)]. The curves above the baseline SAS tension indicate the effect of increasing ΔR in 0.25 Å increments from 0.25 to 1.25 Å [Eq. (17)]. $\Delta R>0$ moves the surface inward. The thick dashed curve corresponds to $\Delta R=1$ Å, for which the surface tension is relatively insensitive to curvature.

pendence of the liquid-vapor interfacial tension. It is curious that the radius locating at this minimum is close to that of the maximum of $G(R)$, which corresponds to the most hydrophobic hard-sphere solute. While the surface heat capacity is positive over the entire size range, it reaches a maximum at solute radii comparable to the position of the minimum in the entropy, suggesting the two are related. Moreover, we may infer that the extrema in the surface entropy and heat capacity are linked to the breakdown of the aqueous network in the vicinity of the hard-sphere solute, as observed in simulation studies linking solute-water correlations to the thermodynamics of hydrophobic hydration (Lazaridis and Paulaitis, 1994).

2. Displacing the surface to describe curvature effects: the Tolman length

More generally, the interface can be located at a radius $R-\Delta R$. The surface tension referred to that surface is

$$\gamma(R;\Delta R)=\frac{\partial\mu_A^{ex}}{\partial[4\pi(R-\Delta R)^2]}=\frac{kT\rho_W G(R)R^2}{2(R-\Delta R)}=\frac{\gamma_{SAS}(R)}{1-\Delta R/R}. \quad (17)$$

Sharp and co-workers (Sharp *et al.*, 1991) suggested that rather than relying solely on the solvent-accessible surface to determine the molecular surface tension, this tension needs to be corrected for the curvature of the molecular interface to reconcile the difference between molecular and macroscopic surface tension. Based on geometric arguments, they proposed that the radius of a water molecule is the length scale over which this correction must be applied. In effect, their work suggests that the van der Waals surface, i.e., $\Delta R=\sigma_{WW}/2=1.4$ Å, provides a superior description of molecular solute hydration (Sharp *et al.*, 1991; Jackson and Sternberg, 1994). A schematic illustration of the van der Waals, solvent-accessible, and curvature-corrected radii of a hard-sphere solute in water is given in Fig. 12. For a methane-sized solute, $\gamma(R=3.3\text{ Å};\Delta R=0.0\text{ Å})=0.300$ kJ/(mol Å^2), which is 30% lower than the macroscopic value, while $\gamma(R=3.3\text{ Å};\Delta R=1.4\text{ Å})=0.521$ kJ/(mol Å^2), which is 20% greater than the macroscopic value. While neither of these two surfaces gives the macroscopic result, they do bracket γ_∞, suggesting the existence of an optimal intermediate value of ΔR for which the surface tension is size independent.

Figure 13 shows how the surface tension varies with ΔR. For solutes larger than 3 Å, using $\Delta R=1$ Å yields a surface tension that is only weakly size dependent. Indeed, $\gamma(R=3.3\text{ Å};\Delta R=1.0\text{ Å})=0.430$ kJ/(mol Å^2) is in excellent agreement with the macroscopic value, suggesting that the geometric estimate of Sharp *et al.* (1991) for the curvature-correction length scale is correct. This argument degenerates, however, when we account for the temperature dependence of the Tolman length.

The Tolman length δ, described in Sec. II.A, can be accessed by the revised SPT through Eqs. (8) and (16),

$$\gamma_{SAS}(R)\sim\gamma_\infty\left(1-\frac{2\delta}{R}\right). \quad (18)$$

Substituting this expression into Eq. (17) yields (Ashbaugh and Paulaitis, 2001)

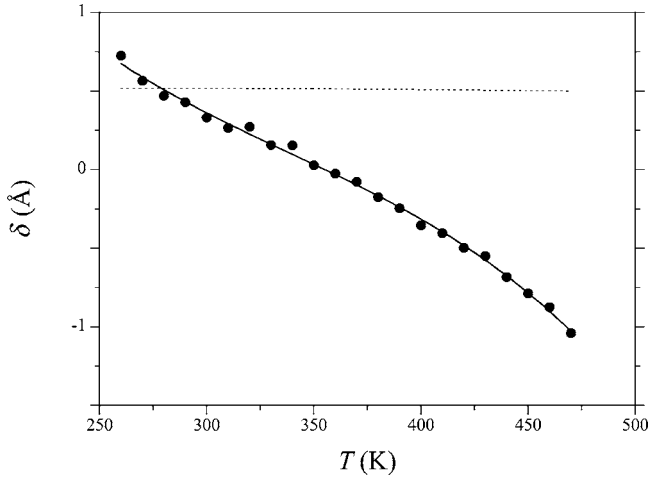

FIG. 14. The curvature correction δ as a function of temperature along the saturation curve of water. The points correspond to the values determined by the fit of Eq. (13) to the simulation free energies. The solid curve is a guide to the eye. The dashed curve corresponds to the classic SPT prediction for the Tolman length, Eq. (10) in Stillinger (1973).

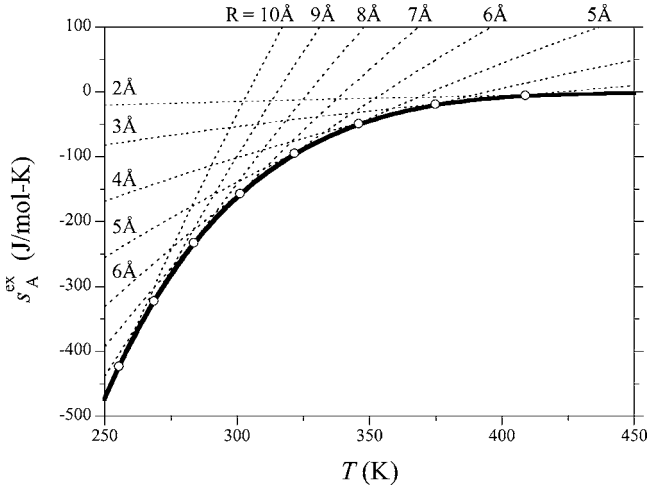

FIG. 15. Entropy of hydrophobic hydration as a function of temperature for solutes in the size range $2<R<10$ Å in 1 Å increments. The dashed lines are excess entropies of hydration. The open circles are convergence temperatures for consecutive solutes, i.e., $s_A^{ex}(R)=s_A^*(R+1\text{ Å})$. The thick solid line indicates the entropy-convergence temperature in the limit of infinitesimal perturbations in R.

$$\gamma(R;\Delta R) \sim \gamma_\infty\left(\frac{1-2\delta/R}{1-\Delta R/R}\right) \tag{19}$$

for the surface tension referenced to a surface displaced by ΔR. Thus for large R the optimal surface for obtaining a size-independent surface free energy is $\Delta R=2\delta$.

3. Temperature dependence of the Tolman length

The Tolman length can be calculated from classic SPT, see Eq. (10) in Stillinger (1973), and yields a nearly temperature-independent $\delta\approx 0.5$ Å, in good agreement with the empirical ΔR at $T=300$ K obtained above. The revised SPT, however, finds that δ is strongly temperature dependent, decreasing with temperature and changing sign near $T=350$ K (see Fig. 14). Moody and Attard (2001) suggested that the Tolman length might also change sign for a Lennard-Jones solvent. Thus assuming ΔR is simply dictated by the size of a water molecule leads to flawed interpretations of the relationship between molecular and macroscopic surface tensions (Sharp *et al.*, 1991; Jackson and Sternberg, 1994). In retrospect, the temperature dependence of the curvature correction might have been anticipated by the entropic differences between hydrating a molecular and mesoscopic interface and the significantly different temperature dependencies of the associated surface thermodynamic properties (see Fig. 11). The curves in Fig. 11 are simply too rich to be described by a temperature-independent length scale.

E. Entropy convergence and solute size

When the hydrophobic component of the hydration entropies of small hydrocarbon molecules is extrapolated to high temperatures, the entropy variations from one solute to another are small in a limited range, $T\approx 400$ K (Privalov, 1979; Baldwin, 1986; Privalov and Gill, 1988; Murphy *et al.*, 1990). This phenomenon of entropy convergence is a feature of hydrophobic hydration believed to be common to both small-molecule hydration and protein-unfolding thermodynamics. Baldwin (1986) and Privalov (1979) noted that this can result from the proportionality of the entropy and heat capacity of hydration to one another. The most successful explanations for the convergence temperature for small molecules have related the convergence temperature to the equation of state of pure water (Garde *et al.*, 1996; Hummer *et al.*, 1998; Garde and Ashbaugh, 2001; Ashbaugh *et al.*, 2002). Huang and Chandler (2000b) argued that for species larger than $R\approx 10$ Å entropy convergence does not occur, and therefore proteins do not exhibit this phenomenon.

1. Hard-sphere hydration entropies over a wide range of sizes

Experimental identifications of entropy convergence, however, have largely concerned themselves with solutes similar in size. In Fig. 15 we have plotted the hydration entropies for hard-sphere solutes as a function of temperature for solutes in the size range $2\leqslant R\leqslant 10$ Å. It is clear that naive entropy convergence is not to be expected with such a wide range of sizes. Specifically, an entropy-convergence temperature extracted by consideration of results for solutes in one limited size range will differ from an entropy-convergence temperature obtained in a different size range. For example, the 2 Å solute entropy intersects the 3 Å solute entropy at $T=410$ K, while the 2 Å solute entropy intersects the 10 Å solute curve at $T=300$ K, indicating that there is no unique convergence temperature.

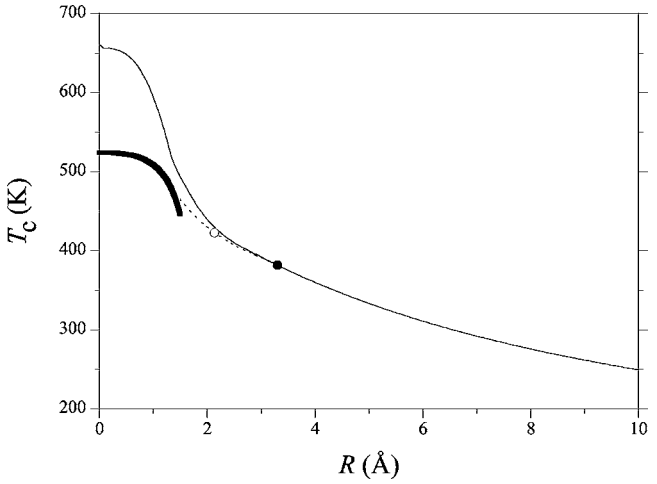

FIG. 16. Variation of the entropy-convergence temperature with increasing hard-sphere radius. The thin solid curve is the convergence temperature determined under the assumption that the heat capacity is independent of temperature. The thick solid curve is the exact entropy-convergence temperature for $R<\sigma_{WW}/2$ from Eq. (22). The dashed curve smoothly interpolates between the exact and constant heat-capacity curves at 1.25 and 3.3 Å, respectively. The filled circle indicates the entropy-convergence temperature of a methane-sized solute ($T_c=382$ K). The open circle indicates the entropy-convergence temperature based on the information theoretic (IT) model criterion ($T_c=420$ K).

2. Differential definition of entropy-convergence temperature

We therefore consider how the convergence temperature changes with differential perturbations in the solute size so that convergence occurs at the temperature for which

$$s_A^{ex}(R+\delta R)=s_A^{ex}(R). \tag{20}$$

Assuming the hydration heat capacity is independent of temperature, T_c is determined by

$$T_c=T_0\exp\left(-\frac{\partial s_A^{ex}(T_0)}{\partial A_{SAS}}\Big/\frac{\partial c_A^{ex}(T_0)}{\partial A_{SAS}}\right), \tag{21}$$

with the size dependence dictated by the relationship between $\partial s_A^{ex}(T_0)/\partial A_{SAS}$ and $\partial c_A^{ex}(T_0)/\partial A_{SAS}$ on the solute radius in Fig. 11. The curve of this convergence entropy as a function of solute radius is shown in Fig. 15. Several points of interest are immediately apparent. First, the convergence entropy is negative and becomes more negative with increasing solute size. Second, the convergence-entropy curve more or less forms a lower bound on the hydration entropy as a function of temperature, although this is approximate. Finally note that much of the complicated, nonmonotonic variation of entropy and heat capacity contributions of Fig. 11 is eliminated by the ratio of Eq. (21).

One of the implications of Eq. (21) is that if the entropy is a linear function of the heat capacity, i.e., $s_A^{ex}(T_0)=mc_A^{ex}(T_0)+b$, as suggested by Baldwin (1986) and by Murphy *et al.* (1990), then the convergence temperature would be independent of solute size. In Fig. 16 we see that T_c has a significant solute-size dependence, indicating that this assumption has limited validity. For solutes approaching zero radius, T_c has a plateau at a maximum. With increasing solute size, T_c decreases so that above $R\approx 8$ Å it is less than the normal freezing point of water. At the intermediate methane radius of 3.3 Å, however, the convergence temperature is 382 K, in excellent agreement with the experimental convergence temperature of $T=385$ K for simple nonpolar gases and linear alkanes.

The convergence temperature exhibits a plateau at $T=655$ K as $R\to 0$, above the critical temperature of water at 647 K. This unphysical result is due in part to our extrapolation of the entropies beyond the range 260–470 K, to which we fitted Eq. (15). For cavities small enough that only one water molecule can fit inside, the free energy is given by Eq. (4), and entropy convergence occurs for the temperature at which

$$\alpha_{sat}T_c=1-\frac{4\pi}{3}\rho_W R^3, \tag{22}$$

where $\alpha_{sat}=-(\partial\ln\rho_W/\partial T)_{sat}$ is the thermal-expansion coefficient of liquid water along the saturation curve. When this criterion is applied, it displays a plateau at a physically more realistic temperature of $T_c\approx 525$ K (see Fig. 16). With increasing solute size, Eq. (22) indicates a sudden decrease in T_c above $R\approx 1$ Å, comparable to that obtained on the assumption that the heat capacity is temperature independent. Above radii of 1.25 Å, Eq. (22) breaks down as multiparticle correlations began to play a role in the solute entropy. At this radius, however, the convergence temperatures are now within the range of temperatures simulated and the application of Eq. (21) becomes more accurate. It is reasonable then to interpolate between the convergence temperatures determined by Eqs. (21) and (22), as indicated in Fig. 16.

The information theory (Garde *et al.*, 1996; Hummer *et al.*, 1998), with natural simplifying assumptions, indicates entropy convergence when $T_c\approx(2\alpha_{sat})^{-1}=420$ K. This corresponds in Fig. 16 to a solute radius of $R\approx 2.1$ Å, placing this estimate among small-solute theories. Relaxing the assumptions used to arrive at this information theory criterion lowers the convergence-temperature prediction for methane-sized solutes to $T\approx 390$ K, improving agreement with the present result of 382 K.

3. Relevance to folding↔unfolding transitions of soluble protein molecules

Equation (22) is an example of the explanation of the entropy-convergence phenomenon that tied it to the particular equation of state of liquid water (Garde *et al.*, 1996; Hummer *et al.*, 1998; Garde and Ashbaugh, 2001; Ashbaugh *et al.*, 2002). That explanation resolved an important conundrum for our molecular understanding of hydrophobic effects. Whether and how this entropy-convergence phenomenon is involved with protein folding is yet an outstanding question. Proteins are compli-

cated molecules participating in both hydrophobic and hydrophilic interactions with the solution. The widely appreciated point that protein-folding thermodynamics may be primarily sensitive to hydration of unfolded configurations is just as important (Paulaitis and Pratt, 2002; Pratt and Pohorille, 2002). Considering unfolded possibilities, the sizes of the obvious hydrophobic units are in the range of small-molecule hydrocarbon solutes. Phenylalanine is the largest hydrophobic side chain and provides an example. Pratt (2002) emphasized that solution thermodynamic data are available for hydrophobic solutes of just this size, e.g., for benzene, toluene, and ethyl benzene (Privalov and Gill, 1989), and those data suggest that these solutes exhibit conventional entropy-convergence behavior. Thus it is a plausible hypothesis that entropy convergence will be expressed in protein-folding thermodynamics primarily through contributions associated with unfolded configurations.

Considering folded configurations, Huang and Chandler (2000b) suggested that the hydration of surface nonpolar groups is better described by the hydration entropy of a solute surface on the scale of the protein radius, $R \approx O(\mathrm{nm})$, rather than treating the surface groups individually as having sizes comparable to simple hydrophobic units. In this hypothesis it is presumed that entropic contributions for hydrating extended hydrophobic surfaces with attractive dispersion interactions and vicinal polar/charged groups are the same as those for a hard repulsive surface. Recent simulations of convex methane clusters have found that when realistic attractive interactions between water and methane are included, water packs around the cluster methane sites just as it does around a solitary methane in solution (Ashbaugh and Paulaitis, 2001; Chau, 2003); similar results are available for a realistically modeled planar aqueous interface (Ashbaugh *et al.*, 2005). Moreover, Cheng and Rossky (1998) found that orientational correlations between water and proximal hydrophobic residues on the convex surfaces of the bee venom protein, melittin, are similar to those near individual solitary hydrophobic groups in solution. These observations suggest that the available configurational space, and thus a contribution to the entropy, for water molecules near realistic surface hydrophobic units is the same in the folded and unfolded states, supporting the assumptions of phenomenological folding models. We note, however, that Cheng and Rossky (1998) also found that water molecules proximal to hydrophobic residues in flat portions of meletin were more orientationally disordered as a result of the difficulties associated with maintaining the aqueous hydrogen-bonding network near restrictive solute topographies. Thus the applicability of the phenomenological unfolding model may be complicated by the protein surface topography and the impact of hydrophobic pockets on the overall unfolding entropy. This can introduce further scatter into measured folding entropies (Robertson and Murphy, 1997).

Examination in Fig. 3 of the aqueous solubilities of the whole family of noble gases suggests that a significant variation of the strength of attractive interactions might contribute to this scatter also. The size variation for which the present work gives numerically exact results is probably not sufficient to explain the lack of simple entropy-convergence behavior observed there. Note, however, that the case of Xe has been recently considered in some detail (Graziano, 2003b; Ben-Amotz *et al.*, 2005).

IV. SUMMARY AND CONCLUSIONS

The revised scaled particle theory bridges the known molecular and macroscopic limits by utilizing simulation information on multibody correlations in liquid water together with experimental thermodynamic properties of pure water to construct a functional form for the hydration free energy of hydrophobic hard-sphere solutes in water. The classic scaled particle theory (Mayer, 1963; Ben-Naim and Friedman, 1967; Stillinger, 1973) incorrectly predicted an increase in the surface tension of water with increasing temperature as well as a temperature-independent Tolman length, neither of which agrees with revised scaled particle theory observations. As a result, application of classic scaled particle theory to hydration free energies is largely a fitting exercise to obtain an effective van der Waals diameter σ_{WW} of water. Conclusions drawn on this basis have weak significance regarding the molecular origins of the hydrophobic effect, and are limited to comparisons of the size parameter for water relative to other solvents, neglecting further molecular detail or specific temperature signatures of hydrophobic hydration.

The revised scaled particle theory is more successful, but the success of the scaled particle approach derives generally from the remarkable fact that the results identify a molecular length, near 3.0 Å, that provides a good joining point for microscopic and macroscopic descriptions. The corresponding results for comparative organic solvents are less simple (Pratt and Pohorille, 1992; Graziano, 2003a). That micro-macro joining radius exhibits interesting temperature variation; an accurate description of those temperature variations is an important part of the higher fidelity of the revised scaled particle results. The revised scaled particle theory reproduces the solubility minimum behavior for small hydrophobic solutes and demonstrates significant changes in the hydration mechanism of hard-sphere solutes with increasing solute size. Specifically, hydration thermodynamics of small solutes is predominantly entropic at room temperature. The hydration of mesoscopic cavities is entropically favorable but opposed by a dominating hydration enthalpy. While it is tempting to describe these changes in hydration thermodynamics in terms of aqueous hydrogen bonding near the hydrophobic entity—and that can be plausible in the appropriate theoretical setting—the scaled particle theory provides little in the way of information on the integrity of hydrogen-bonded networks.

Nevertheless, the revised scaled particle theory does provide thermodynamic information that challenges phenomenological views of hydrophobic effects, particu-

larly the iceberg hypothesis. Whereas the iceberg hypothesis suggests that local freezing of water molecules in the vicinity of hydrophobic solutes is a source for negative hydration enthalpies, we find that at room temperature the hydration of solutes comparable in size to simple nonpolar gases is actually unfavorable from an enthalpic as well as an entropic standpoint. Experimentally determined favorable enthalpies of solution of hydrophobic species then are a consequence of attractive solute-water interactions and not enhanced water-water structuring.

On a molecular level there is a surface that maps macroscopic surface tensions to molecular values. This reduces the reconciliation of molecular and macroscopic values of the surface tension to a program of finding the appropriate dividing surface. The utility of that program rests on the optimistic expectation that the Tolman length locating that surface is largely temperature independent. But that Tolman length was found to have a significant temperature dependence in water, changing from positive to negative at $T \approx 350$ K, a possibility anticipated by Stillinger (1973). As a result, though the optimal surface for the description of hydration may be approximated by the solute molecular surface at low temperatures (Ashbaugh *et al.*, 1999; Ashbaugh and Paulaitis, 2001), with increasing temperature this optimal surface moves out to the solvent-accessible surface at $T \approx 350$ K, and ultimately extends beyond this surface at even higher temperatures as a result of the nontrivial temperature dependence of the hydration thermodynamics for molecular-sized solutes.

Finally, the revised scaled particle theory provides detailed information on the entropy-convergence behavior observed for small-molecule solutes and on the size dependence of the convergence temperature. A suitably defined differential entropy-convergence temperature retreats below the freezing temperature of water for hard spheres the size of globular soluble proteins. But heterogeneity of protein-water interactions and of sizes of hydrophobic units also contribute importantly to experimental blurring of entropy-convergence behavior in protein-unfolding thermodynamic data. Equally important, entropy convergence behavior for protein-folding thermodynamics may be primarily expressed through contributions associated with the unfolded configurations and is due to hydration of hydrophobic side chains of size corresponding to studied small-molecule solutes.

ACKNOWLEDGMENTS

This work was supported by the U.S. Department of Energy, Contract No. E-7405-ENG-36. This research has benefited from conversations with D. Asthigiri, A. E. García, S. Garde, G. Hummer, M. E. Paulaitis, and A. Pohorille. We also thank J. R. Henderson and R. Evans for their insightful remarks with respect to the wetting of interfaces.

REFERENCES

Alejandre, J., D. J. Tildesley, and G. A. Chapela, 1995, J. Chem. Phys. **102**, 4574.
Ashbaugh, H. S., D. Asthagiri, L. R. Pratt, and S. B. Rempe, 2003, Biophys. Chem. **105**, 323.
Ashbaugh, H. S., E. W. Kaler, and M. E. Paulaitis, 1999, J. Am. Chem. Soc. **121**, 9243.
Ashbaugh, H. S., and M. E. Paulaitis, 2001, J. Am. Chem. Soc. **123**, 10721.
Ashbaugh, H. S., L. R. Pratt, M. E. Paulaitis, J. Clohecy, and T. L. Beck, 2005, J. Am. Chem. Soc. **127**, 2808.
Ashbaugh, H. S., T. M. Truskett, and P. G. Debenedetti, 2002, J. Chem. Phys. **116**, 2907.
Baldwin, R. L., 1986, Proc. Natl. Acad. Sci. U.S.A. **83**, 8069.
Barker, J. A., and D. Henderson, 1976, Rev. Mod. Phys. **48**, 587.
Ben-Amotz, D., F. O. Raineri, and G. Stell, 2005, J. Phys. Chem. B **109**, 6866.
Ben-Naim, A., and H. L. Friedman, 1967, J. Phys. Chem. **71**, 448.
Ben-Naim, A., and Y. Marcus, 1984, J. Chem. Phys. **81**, 2016.
Berendsen, H. J. C., J. R. Grigera, and T. P. Straatsma, 1987, J. Phys. Chem. **91**, 6269.
Blokzijl, W., and J. B. F. N. Engberts, 1993, Angew. Chem., Int. Ed. Engl. **32**, 1545.
Bowron, D. T., A. Filipponi, C. Lobban, and J. L. Finney, 1998, Chem. Phys. Lett. **293**, 33.
Bowron, D. T., A. Filipponi, M. A. Roberts, and J. L. Finney, 1998, Phys. Rev. Lett. **81**, 4164.
Brandts, J. F., 1964, J. Am. Chem. Soc. **86**, 4291.
Broadbent, R. D., and G. W. Neilson, 1994, J. Chem. Phys. **100**, 7543.
Chandler, D., 1993, Phys. Rev. E **48**, 2898.
Chandler, D., J. D. Weeks, and H. C. Andersen, 1983, Science **220**, 787.
Chau, P. L., 2003, Mol. Phys. **101**, 3121.
Chen, L. J., S. Y. Lin, and C. C. Huang, 1998, J. Phys. Chem. B **102**, 4350.
Chen, L. J., S. Y. Lin, C. C. Huang, and E. M. Chen, 1998, Colloids Surf., A **135**, 175.
Cheng, Y. K., and P. J. Rossky, 1998, Nature **392**, 696.
Choudhury, N., and B. M. Pettitt, 2005, J. Am. Chem. Soc. **127**, 3556.
Christenson, H. K., and P. M. Claesson, 1988, Science **239**, 390.
Clever, H. L., 1979a, Ed., *Solubility Data Series: Helium and Neon* (Pergamon, New York), Vol. 1.
Clever, H. L., 1979b, Ed., *Solubility Data Series: Krypton, Xenon, and Radon* (Pergamon, New York), Vol. 2.
Clever, H. L., 1980, Ed., *Solubility Data Series: Argon* (Pergamon, New York), Vol. 4.
Considine, R. F., R. A. Hayes, and R. G. Horn, 1999, Langmuir **15**, 1657.
DeJong, P. H. K., J. E. Wilson, G. W. Neilson, and A. D. Buckingham, 1997, Mol. Phys. **91**, 99.
Dzubiella, J., and J. P. Hansen, 2003, J. Chem. Phys. **119**, 12049.
Egelstaff, P. A., and B. Widom, 1970, J. Chem. Phys. **53**, 2667.
Evans, R., J. R. Henderson, and R. Roth, 2004, J. Chem. Phys. **121**, 12074.
Evans, R., R. Roth, and P. Bryk, 2003, Europhys. Lett. **62**, 815.
Filipponi, A., D. T. Bowron, C. Lobban, and J. L. Finney, 1997, Phys. Rev. Lett. **79**, 1293.

Frank, H. S., and M. W. Evans, 1945, J. Chem. Phys. **13**, 507.
Franks, F., and R. H. M. Hatley, 1991, Pure Appl. Chem. **63**, 1367.
Frenkel, D., and B. Smit, 2002, *Understanding Molecular Simulation. From Algorithms to Applications*, 2nd ed. (Academic, San Diego).
Gallicchio, E., M. M. Kubo, and R. M. Levy, 2000, J. Phys. Chem. B **104**, 6271.
Garde, S., and H. S. Ashbaugh, 2001, J. Chem. Phys. **115**, 977.
Garde, S., A. E. García, L. R. Pratt, and G. Hummer, 1999, Biophys. Chem. **78**, 21.
Garde, S., G. Hummer, A. E. García, M. E. Paulaitis, and L. R. Pratt, 1996, Phys. Rev. Lett. **77**, 4966.
Gill, S. J., S. F. Dec, G. Olofsson, and I. Wadso, 1985, J. Phys. Chem. **89**, 3758.
Gomez, M. A., L. R. Pratt, G. Hummer, and S. Garde, 1999, J. Phys. Chem. B **103**, 3520.
Graziano, G., 2003a, Biophys. Chem. **104**, 393.
Graziano, G., 2003b, Biophys. Chem. **105**, 371.
Graziano, G., and B. Lee, 2003, Biophys. Chem. **105**, 241.
Hare, D. E., and C. M. Sorensen, 1986, J. Chem. Phys. **84**, 5085.
Henderson, J. R., 2002, J. Chem. Phys. **116**, 5039.
Henderson, J. R., and F. van Swol, 1988, J. Chem. Phys. **89**, 5010.
Hermann, R. B., 1977, Proc. Natl. Acad. Sci. U.S.A. **74**, 4144.
Huang, D. M., and D. Chandler, 2000a, Phys. Rev. E **61**, 1501.
Huang, D. M., and D. Chandler, 2000b, Proc. Natl. Acad. Sci. U.S.A. **97**, 8324.
Huang, D. M., P. L. Geissler, and D. Chandler, 2001, J. Phys. Chem. B **105**, 6704.
Huang, X., C. J. Margulis, and B. J. Berne, 2003, Proc. Natl. Acad. Sci. U.S.A. **100**, 11953.
Hummer, G., and S. Garde, 1998, Phys. Rev. Lett. **80**, 4193.
Hummer, G., S. Garde, A. E. García, M. E. Paulaitis, and L. R. Pratt, 1998, J. Phys. Chem. B **102**, 10469.
Hummer, G., S. Garde, A. E. García, and L. R. Pratt, 2000, Chem. Phys. **258**, 349.
Hummer, G., J. C. Rasaiah, and J. P. Noworyta, 2001, Nature **414**, 188.
Hura, G., D. Russo, R. M. Glaeser, T. Head-Gordon, M. Krack, and M. Parrinello, 2003, Phys. Chem. Chem. Phys. **5**, 1981.
Israelachvili, J., and R. Pashley, 1982, Nature **300**, 341.
Jackson, R. M., and M. J. E. Sternberg, 1994, Protein Eng. **7**, 371.
Kauzmann, W., 1959, Adv. Protein Chem. **14**, 1.
Kokkoli, E., and C. F. Zukoski, 1998, Langmuir **14**, 1189.
Lazaridis, T., and M. E. Paulaitis, 1992, J. Phys. Chem. **96**, 3847.
Lazaridis, T., and M. E. Paulaitis, 1994, J. Phys. Chem. **98**, 635.
Lebowitz, J. L., and E. M. Waisman, 1980, Phys. Today **33** (3), 24.
Lee, B., 1985, Biopolymers **24**, 813.
Lee, B., 1991, Proc. Natl. Acad. Sci. U.S.A. **88**, 5154.
Li, L., D. Bedrov, and G. D. Smith, 2005, Phys. Rev. E **71**, 011502.
Lum, K., D. Chandler, and J. D. Weeks, 1999, J. Phys. Chem. B **103**, 4570.
Makhatadze, G. I., and P. L. Privalov, 1995, Adv. Protein Chem. **47**, 307.
Mayer, S. W., 1963, J. Phys. Chem. **67**, 2160.
Moody, M. P., and P. Attard, 2001, J. Chem. Phys. **115**, 8967.
Muller, N., 1993, Biopolymers **33**, 1185.
Murphy, K. P., P. L. Privalov, and S. J. Gill, 1990, Science **247**, 559.
Naghibi, H., S. F. Dec, and S. J. Gill, 1986, J. Phys. Chem. **90**, 4621.
Paschek, D., 2005, Phys. Rev. Lett. **94**, 217802.
Pashley, R. M., 2003, J. Phys. Chem. B **107**, 1714.
Pashley, R. M., P. M. McGuiggan, B. W. Ninham, and D. F. Evans, 1985, Science **229**, 1088.
Pashley, R. M., M. Rzechowicz, L. R. Pashley, and M. J. Francis, 2005, J. Phys. Chem. B **109**, 1231.
Paulaitis, M. E., and L. R. Pratt, 2002, in *Advances in Protein Chemistry: Unfolded Proteins* (Academic, New York), Vol. 62, p. 283.
Pierotti, R. A., 1976, Chem. Rev. (Washington, D.C.) **76**, 717.
Pohorille, A., and L. R. Pratt, 1990, J. Am. Chem. Soc. **112**, 5066.
Pratt, L., G. Hummer, and S. Garde, 1999, in *New Approaches to Problems in Liquid State Theory*, edited by C. Caccamo, J.-P. Hansen, and G. Stell, Vol. 529 of NATO Science Series (Kluwer, Dordrecht), pp. 407–420.
Pratt, L. R., 1998, in *Encyclopedia of Computational Chemistry* (Wiley, Chichester), p. 1286.
Pratt, L. R., 2002, Annu. Rev. Phys. Chem. **53**, 409.
Pratt, L. R., and D. Chandler, 1977, J. Chem. Phys. **67**, 3863.
Pratt, L. R., and A. Pohorille, 1992, Proc. Natl. Acad. Sci. U.S.A. **89**, 2995.
Pratt, L. R., and A. Pohorille, 1993, in *Proceedings of the EBSA 1992 International Workshop on Water-Biomolecule Interactions*, edited by M. U. Palma, M. B. Palma-Vittorelli, and F. Parak (Societá Italiana de Fisica, Bologna), p. 261.
Pratt, L. R., and A. Pohorille, 2002, Chem. Rev. (Washington, D.C.) **102**, 2671.
Privalov, P. L., 1979, Adv. Protein Chem. **33**, 167.
Privalov, P. L., and S. J. Gill, 1988, Adv. Protein Chem. **39**, 191.
Privalov, P. L., and S. J. Gill, 1989, Pure Appl. Chem. **61**, 1097.
Reiss, H., 1965, Adv. Chem. Phys. **9**, 1.
Reiss, H., 1977, in *Statistical Mechanics and Statistical Methods in Theory and Application*, edited by U. Landman (Plenum, New York), pp. 99–138.
Reiss, H., H. L. Frisch, and J. L. Lebowitz, 1959, J. Chem. Phys. **31**, 369.
Rettich, T. R., Y. P. Handa, R. Battino, and E. Wilhelm, 1981, J. Phys. Chem. **85**, 3230.
Robertson, A. D., and K. P. Murphy, 1997, Chem. Rev. (Washington, D.C.) **97**, 1251.
Scatena, L. F., M. G. Brown, and G. L. Richmond, 2001, Science **292**, 908.
Sharp, K. A., A. Nichols, R. F. Fine, and B. Honig, 1991, Science **252**, 106.
Silverstein, K. A. T., K. A. Dill, and A. D. J. Haymet, 2001, J. Chem. Phys. **114**, 6303.
Simonson, T., 2003, Rep. Prog. Phys. **66**, 737.
Southall, N. T., and K. A. Dill, 2000, J. Phys. Chem. B **104**, 1326.
Spolar, R. S., J. H. Ha, and M. T. Record, 1989, Proc. Natl. Acad. Sci. U.S.A. **86**, 8382.
Spolar, R. S., and M. T. Record, 1994, Science **263**, 777.
Stell, G., 1985, in *The Wonderful World of Stochastics: A Tribute to Elliot W. Montroll*, edited by M. F. Shlesinger and G. H. Weiss, Vol. XII of Studies in Statistical Mechanics (Elsevier, New York), pp. 127–156.
Stillinger, F. H., 1973, J. Solution Chem. **2**, 141.

Stillinger, F. H., and M. A. Cotter, 1971, J. Chem. Phys. **55**, 3449.
Tanford, C., 1979, Proc. Natl. Acad. Sci. U.S.A. **76**, 4175.
Tanford, C., 1980, *The Hydrophobic Effect: Formation of Micelles and Biological Membranes*, 2nd ed. (Wiley, New York).
Tolman, R. C., 1949, J. Chem. Phys. **17**, 333.
Truskett, T. M., P. G. Debenedetti, and S. Torquato, 2001, J. Chem. Phys. **114**, 2401.
Tully-Smith, D. M., and H. Reiss, 1970, J. Chem. Phys. **53**, 4015.
van Swol, F., and J. R. Henderson, 1986, J. Chem. Soc., Faraday Trans. 2 **82**, 1685.
Wallqvist, A., E. Gallicchio, and R. M. Levy, 2001, J. Phys. Chem. B **105**, 6745.
Weeks, J. D., K. Katsov, and K. Vollmayr, 1998, Phys. Rev. Lett. **81**, 4400.
Widom, B., 1967, Science **157**, 375.
Widom, B., 1982, J. Phys. Chem. **86**, 869.
Zhou, R. H., X. H. Huang, C. J. Margulis, and B. J. Berne, 2004, Science **305**, 1605.